AMERICAN SOCIETY FOR MICROBIOLOGY | Journal of Virology®

VIRUS-CELL INTERACTIONS

The C-Terminal Domain of Salmonid Alphavirus Nonstructural Protein 2 (nsP2) Is Essential and Sufficient To Block RIG-I Pathway Induction and Interferon-Mediated Antiviral Response

Raphaël Jami,[a] Emilie Mérour,[a] Julie Bernard,[a] Annie Lamoureux,[a] Jean K. Millet,[a] Stéphane Biacchesi[a]

[a]Université Paris-Saclay, INRAE, UVSQ, Virologie et Immunologie Moléculaires, Jouy-en-Josas, France

ABSTRACT Salmonid alphavirus (SAV) is an atypical alphavirus that has a considerable impact on salmon and trout farms. Unlike other alphaviruses, such as the chikungunya virus, SAV is transmitted without an arthropod vector, and it does not cause cell shutoff during infection. The mechanisms by which SAV escapes the host immune system remain unknown. By studying the role of SAV proteins on the RIG-I signaling cascade, the first line of defense of the immune system during infection, we demonstrated that nonstructural protein 2 (nsP2) effectively blocks the induction of type I interferon (IFN). This inhibition, independent of the protease activity carried by nsP2, occurs downstream of IRF3, which is the transcription factor allowing the activation of the IFN promoter and its expression. The inhibitory effect of nsP2 on the RIG-I pathway depends on the localization of nsP2 in the host cell nucleus, which is linked to two nuclear localization sequences (NLS) located in its C-terminal part. The C-terminal domain of nsP2 by itself is sufficient and necessary to block IFN induction. Mutation of the NLS of nsP2 is deleterious to the virus. Finally, nsP2 does not interact with IRF3, indicating that its action is possible through a targeted interaction within discrete areas of chromatin, as suggested by its punctate distribution observed in the nucleus. These results therefore demonstrate a major role for nsP2 in the control by SAV of the host cell's innate immune response.

IMPORTANCE The global consumption of fish continues to rise, and the future demand cannot be met by capture fisheries alone due to limited stocks of wild fish. Aquaculture is currently the world's fastest-growing food production sector, with an annual growth rate of 6 to 8%. Recurrent outbreaks of SAV result in significant economic losses with serious environmental consequences for wild stocks. While the clinical and pathological signs of SAV infection are fairly well known, the molecular mechanisms involved are poorly described. In the present study, we focus on the nonstructural protein nsP2 and characterize a specific domain containing nuclear localization sequences that are critical for the inhibition of the host innate immune response mediated by the RIG-I pathway.

KEYWORDS salmonid, alphavirus, SAV2, nsP2, RIG-I, interferon

Sleeping disease (SD) causes important losses in European salmon and trout aquaculture. SD in salmonids was first observed in France in 1985 (1). It is a very contagious viral disease that has been listed since 2014 as notifiable by the World Organization for Animal Health (OIE) (2). A viral etiology of this disease has been established, and the virus was characterized as the first alphavirus (*Togaviridae* family) isolated from diseased fish (3). A genetically related virus, the salmon pancreas disease virus (SPDV), was also characterized in salmon (4). These viruses are now classified as salmonid alphavirus (SAV), with at least six main subtypes (SAV subtypes 1 to 6), where SAV1 is SPDV infecting salmon, SAV2 is sleeping disease virus (SDV) infecting trout,

Citation Jami R, Mérour E, Bernard J, Lamoureux A, Millet JK, Biacchesi S. 2021. The C-terminal domain of salmonid alphavirus nonstructural protein 2 (nsP2) is essential and sufficient to block RIG-I pathway induction and interferon-mediated antiviral response. J Virol 95:e01155-21. https://doi.org/10.1128/JVI.01155-21.

Editor Mark T. Heise, University of North Carolina at Chapel Hill

Address correspondence to Stéphane Biacchesi, stephane.biacchesi@inrae.fr.

Received 8 July 2021
Accepted 9 September 2021
Accepted manuscript posted online 15 September 2021
Published 9 November 2021

and SAV3 is the Norwegian subtype infecting both salmon and trout (5). Like all alphaviruses, SAV are enveloped, with a genome consisting of a single positive-strand RNA molecule of approximately 12 kb. The alphavirus genome encodes two polyproteins, which after proteolytic processing by cellular and viral proteases produce the mature viral proteins. The nonstructural proteins nsP1, nsP2, nsP3, and nsP4 are involved in replication of the viral genome and transcription of subgenomic RNA encoding the structural proteins (sP), namely the capsid (C) and two main envelope glycoproteins (E2 and E1) (6).

Interestingly, genome-wide evolutionary analyses suggest that terrestrial alphaviruses have an ancestral marine origin, and SAV are positioned basally in the *Alphavirus* genus phylogeny, close to the root of the tree (7). Despite broadly sharing many characteristics with their terrestrial counterparts (e.g., genome organization), SAVs have distinct features, such as longer protein lengths and shorter noncoding regions at the 5′ and 3′ ends of the genome (3, 4). In addition, even if the existence of a vector is not excluded, SAVs do not appear to require an arthropod vector to be transmitted, unlike most terrestrial alphaviruses. Knowledge of the determinants for SAV virulence is still limited, with many of the functions of each viral protein inferred from those of terrestrial alphavirus proteins. To date, virulence determinants in trout have only been shown in the E2 glycoprotein of SAV2 (8, 9).

In rainbow trout, the disease is characterized by an abnormal swimming behavior of the fish, which stay on their side at the bottom of tanks, hence the name "sleeping" disease (1, 10). This clinical sign is due to destruction of the exocrine pancreas and to extensive necrosis and atrophy of skeletal muscles induced by SAV2 infection (10, 11). The cumulative mortality at the farm level ranges from negligible to over 60% in severe cases (12). SAV infection also results in skin dysbiosis, rendering the host more susceptible to secondary bacterial infections and thus requiring antibiotic treatments (13). High incidences of cases of SAV were reported over the last decade in Norway and represent a challenge to the Norwegian salmon industry. A total of 152 farms were identified as being infected by SAV3 and SAV2 in 2019 (14). Although mortalities are relatively low, SAV3 infection in Atlantic salmon results in reduction of growth and affects feed conversion and product quality, thereby leading to heavy economic losses. Moreover, detection of SAV3 in a facility can result in livestock culling to prevent further spread of the disease, since survivors may become asymptomatic carriers of infection (2). SAV transmits horizontally from fish shedding virus directly into the water. Ocean or river currents are believed to be main contributors of viral spread between farms. A marine reservoir of the virus is also suspected, since SAV RNA has been detected in marine fish species caught in areas remotely located from salmon farms, rendering the eradication of SAV in salmonid farms very difficult (12, 15). Commercial vaccines against SAV3 in the form of injectable preparations of adjuvanted inactivated virus or DNA are available. However, vaccination against SAV3 in marine farms in Norway has not provided complete protection (16, 17). In the Norwegian Fish Health Report from 2019, marine SAV2 and SAV3 are described as viral diseases that remain endemic threats to salmonid aquaculture (14). Despite vaccination programs, SAV is becoming increasingly predominant in the field, and the eradication of this pathogen is a challenge for most fish farms. In fact, vaccination against SAV3 does not prevent fish infection but only reduces disease severity and viral shedding from infected individuals (16). More recently, a DNA vaccine was authorized in Europe, but more field trial data are necessary to estimate its efficacy.

In fish, like in mammals, the main antiviral innate immune mechanism is centered around type I interferon (IFN) production (18, 19). The IFN system is remarkably well conserved in vertebrates. Teleost fish possess functional orthologs of pattern recognition receptors (PRRs), such as retinoic acid-inducible gene I (RIG-I)-like receptors (RLRs) and Toll-like receptors (TLR) (20, 21). The pathogen components, such as nucleic acids and viral proteins, are sensed by PRRs, leading to the activation of multiple signaling cascades that induce the production of IFN and other cytokines. Among the PRRs, RLRs

play a key role in sensing viral RNA in the cytosol and are essential in the early induction of type I IFN. Because of the important role of this pathway in early interferon expression, fish viruses have evolved multiple strategies to evade host RLR-mediated signaling (22, 23). For alphaviruses in higher vertebrates, the type I IFN-dependent innate immune response is essential for host protection (24). The ability of IFNs to restrict alphavirus replication in mammals is largely mediated through the induction of interferon-stimulated genes (ISGs), and the RLR pathway plays a key role in the early detection of alphavirus infections. In line with this, upregulation of type I IFNs and ISGs during SAV challenges in salmonids have been reported previously (25–27). All of these studies point to the importance of IFNs for host defense against SAV, as a first line of innate immune defense in naive fish. This is supported by data showing a direct antiviral effect of type I IFN against SAV3 in salmon cell lines (28, 29). However, no data are available on the mechanisms used by SAV for subverting the innate immune detection and the induction of interferon responses. Here, we report that SAV2 nsP2 strongly antagonizes RIG-I mediated type I interferon induction by blocking IRF3 signaling. These results demonstrate a major role for SAV nsP2 in order to control the host cell's innate immune response.

RESULTS

nsP2 is a strong inhibitor of IFN and ISG induction in fish cells. To determine which SAV2 nonstructural proteins are potentially involved in the inhibition of the cellular antiviral response, we first tested whether these proteins contribute to the inhibition of RIG-I-mediated type I IFN signaling by using a cell-based luciferase reporter system (Fig. 1A). As shown in Fig. 1B, expression of a constitutively active form of RIG-I (RIG-I N-terminal domain [RIG-I Nter]) significantly activated the IFN1 promoter, whereas coexpression of nsP2 with the RIG-I Nter strongly reduced the induction of reporter expression mediated by this promoter, a reduction as robust as that observed with A20, a well-described cellular inhibitor of this pathway that targets TBK1 (30). nsP3 also has an inhibitory effect on the RIG-I pathway, although to a lesser extent than nsP2. In contrast, the coexpression of nsP1 or nsP4 and the RIG-I Nter had no effect on the induction of the promoter, indicating a specific and antagonistic role for nsP2 and nsP3 in RIG-I signaling. We next tested whether nonstructural proteins affect the activation of an interferon-stimulated response element (ISRE)-mediated reporter expression stimulated by IFN1 addition in the supernatant of EPC cells (Fig. 1C). As shown in Fig. 1D, the addition of IFN1 activated the ISRE promoter, and the simultaneous expression of a C-terminally deleted form of STAT1 (STAT1ΔCter), a dominant negative form of STAT1, suppressed the induction of the ISRE promoter. Similarly, nsP2 expression was sufficient to significantly block ISRE promoter activation by IFN1 (Fig. 1D). In contrast, neither nsP1, nsP3, nor nsP4 proteins had any significant effects, demonstrating a specific and negative effect of nsP2 on this pathway. Under all conditions tested, promoter activities were normalized to the levels of enhanced green fluorescent protein (eGFP) fluorescence expressed alone or in fusion to RIG-I Nter. In all cases, no significant variation in eGFP expression could be observed, indicating that the nsP2 inhibition effect on both RIG-I and IFN1 pathways is likely due to a direct effect on a component of these pathways and is not an indirect effect on protein expression levels. This is in contrast to what has been described for the nsP2 of Old-World alphaviruses, which is known to contribute to a global transcriptional cellular shutoff (31–33). For the rest of this study, we focused on nsP2 because it showed the most drastic effect of all SAV2 nonstructural proteins tested for both RIG-I and IFN1 pathways.

nsP2 protease activity is not required to block RIG-I-mediated IFN induction. Since nsP2 functions as a papain-like cysteine protease that processes the nonstructural polyprotein into functional nonstructural proteins (nsP) (34–37), we next tested whether its proteolytic processing activity is required to antagonize the RIG-I pathway. The catalytic dyad of nsP2, consisting of the residues cysteine 480 (C480) and histidine 550 (H550), is well conserved among alphaviruses (Fig. 2A) (38). Both residues were mutated to alanine (A) residues. Mutation of both catalytic residues of SAV2 nsP2

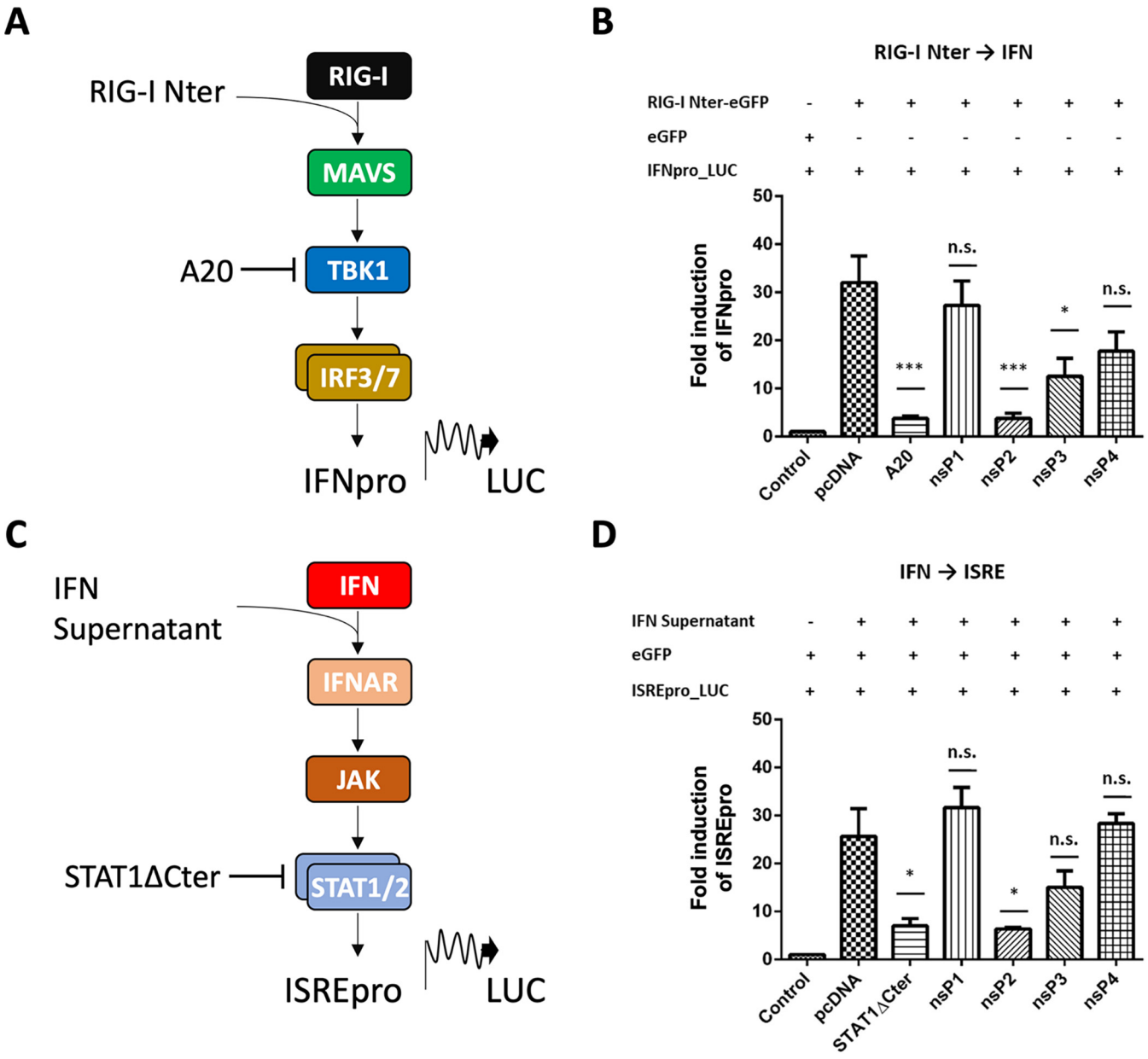

FIG 1 SAV2 nsP2 protein blocks RIG-I-induced activation of IFN1 and ISRE promoter. (A and C) Schematic representations of the RIG-I pathway leading to the induction of type-I IFN and the IFN I pathway leading to interferon-stimulated gene (ISG) expression. Direct activation of these pathways was carried out by transfection of a constitutively activated form of RIG-I (RIG-I-Nter) or by addition of supernatants containing IFN1, respectively. For each pathway, an inhibitor (A20 or STAT1ΔCter, respectively) is mentioned together with its target. (B and D) EPC cells were transfected with the indicated plasmids (1 μg) together with luciferase reporter constructs (1 μg) driven by IFN1 (B) or ISRE promoters (D) and using RIG-I Nter-enhanced green fluorescent protein (eGFP) as an inducer (1 μg) (B) or stimulated by IFN1-containing supernatant (D). At 48 h after transfection and incubation at 14°C (B) or 20°C (D), the cells were lysed for luciferase assays. Luciferase activity was measured and normalized to eGFP fluorescence expressed in fusion to the RIG-I N terminus (B) or from an additional peGFP plasmid (D). Fold inductions were calculated as the ratio of stimulated (+RIG-I-Nter or +IFN1) versus unstimulated (control; −RIG-I-Nter or −IFN1) samples. Averages of at least three independent experiments are shown together with standard errors. Groups that are not significantly different from the pcDNA control condition are denoted by "n.s." ($P > 0.05$), whereas those that are significantly different are denoted by * ($P < 0.05$) or *** ($P < 0.001$).

(double mutant nsP2pmut) does not impact its capacity to inhibit RIG-I Nter induction of the IFN1 promoter (Fig. 2B). In addition, both nsP2 and nsP2pmut proteins abrogate the activation of TBK1. As shown in Fig. 2C, the expression of TBK1 activated the IFN1 promoter, but coexpression of nsP2 or nsP2pmut significantly suppressed induction of the IFN1 promoter mediated by TBK1, suggesting that nsP2 protease activity is not required for blocking the RIG-I pathway.

nsP2 accumulates in the nucleus. Since nsP2 appears to negatively regulate antiviral signaling at the level or downstream of TBK1 (Fig. 2C), we studied the subcellular

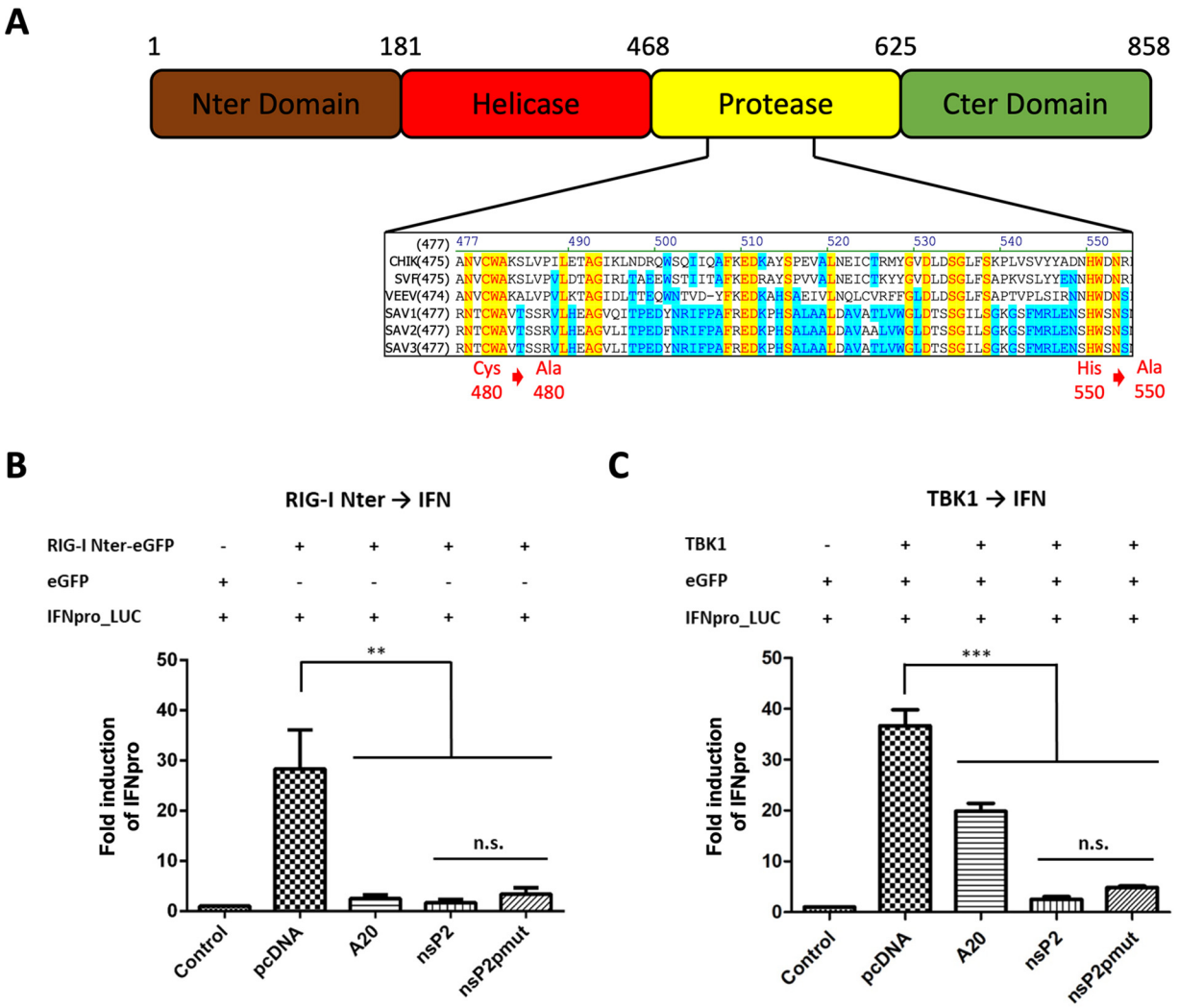

FIG 2 The protease domain of nsP2 protein is not implicated in blocking IFN1 promoter activation. (A) Schematic representation of SAV2 nsP2 protein domains. Multiple alignment of alphavirus nsP2 papain-like cysteine protease domain for the amino acid sequence containing the conserved alphavirus nsP2 protease catalytic dyad consisting of residues C480 and H550 (SAV2 numbering). These active-site residues are completely conserved among members of the *Alphavirus* genus. Both C480 and H550 were mutated to alanine ("A") residues, leading to nsP2pmut. (B and C) EPC cells were transfected with the indicated plasmids (1 μg) together with the IFN1 promoter luciferase reporter plasmid (1 μg) and either RIG-I Nter-eGFP (B) or TBK1 (C) as inducers (1 μg). At 48 h after transfection and incubation at 14°C, the cells were lysed for luciferase assays. Luciferase activity was measured and normalized to eGFP fluorescence. Fold inductions were calculated as the ratio of stimulated (+RIG-I-Nter or +TBK1) versus unstimulated (control; −RIG-I-Nter or −TBK1) samples. Averages of at least three independent experiments are shown together with standard errors. Groups that are not significantly different are denoted by "n.s." ($P > 0.05$), whereas those that are significantly different are denoted by *** ($P < 0.001$).

localization of nsP2 by immunofluorescence assays in transfected EPC cells. To detect nsP2 by immunofluorescence, a triple Flag tag was fused in frame with the N-terminal end of nsP2. The presence of this additional epitope tag sequence had no significant effect on the nsP2 antagonistic function on the RIG-I pathway (data not shown). When expressed alone, nsP2 was mainly observed in the nucleus (Fig. 3A). A similar localization of nsP2 was found in BF-2 cells, a SAV2-permissive cell line (Fig. 3B). In the nuclei of both cell lines, a punctate distribution was observed, suggesting an accumulation of nsP2 at specific areas within the chromatin. Interestingly, nsP2 accumulation in the nuclei led to the formation of blebs at the surface of nuclear envelopes (Fig. 3C and D). These blebs were of different sizes, shapes, and numbers in each nucleus, but regardless of the morphology of these protruding structures, they were all devoid of nuclear DNA 4′,6-diamidino-2-phenylindole (DAPI) staining.

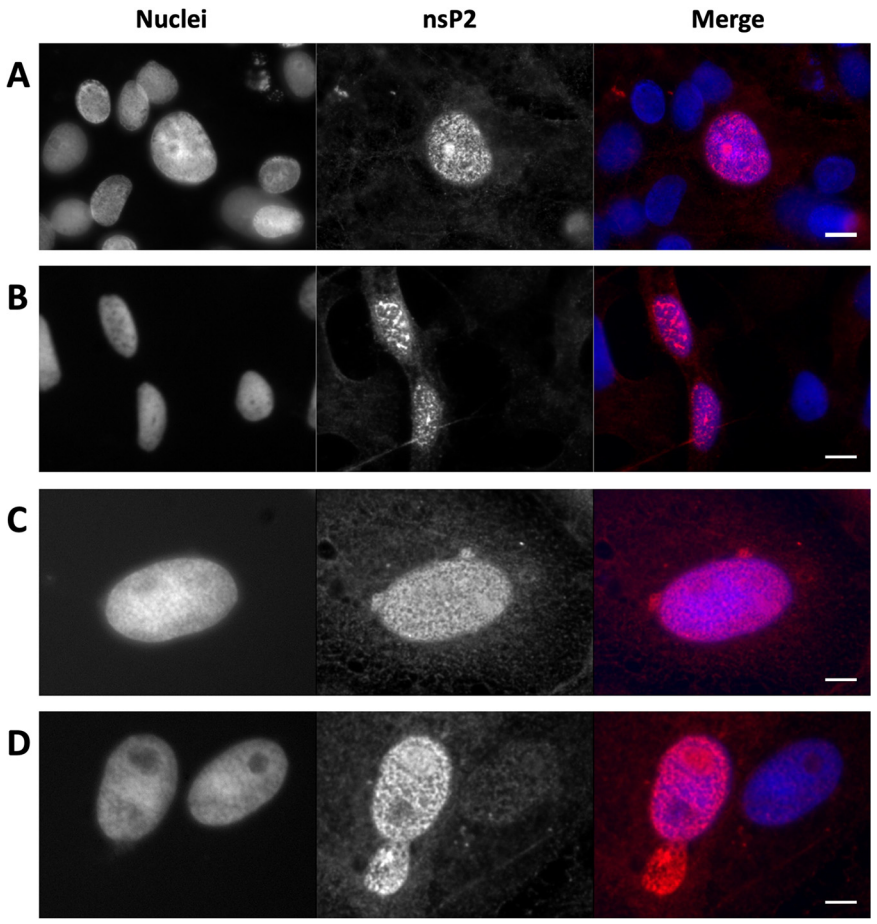

FIG 3 nsP2 localizes to the nucleus in both EPC and BF-2 cells. EPC (A, C, and D) or BF-2 (B) cells were transfected with 0.5 μg of an expression vector encoding nsP2 fused to and in frame with a 3×Flag epitope tag, incubated for 48 h at 14°C, then fixed. nsP2 proteins were detected using anti-Flag monoclonal antibody (MAb) (red). Nuclear DNA was stained using 4′,6-diamidino-2-phenylindole (DAPI; blue). (C and D) Nuclear blebs formed at the surface of the nuclear envelope of nsP2-positive nuclei. These blebs are of different sizes and numbers. Bars, 5 μm.

Structural model of SAV2 nsP2 by template-based structural modeling and nuclear localization signal prediction. To delineate the functional domains of SAV2 nsP2, a model of the protein structure was generated using the RaptorX server, which provides high-quality template-based structural models even when only distantly related templates are available. The RaptorX server also allows for functional annotations, domain parsing, and prediction of disordered regions. The analysis using SAV2 nsP2 amino acid sequence generated a model based on 100% of residues that was predicted to have two main domains with an overall unnormalized global distance test (uGDT) score of 612, which measures the absolute model quality (Fig. 4A). For a protein with more than 100 residues, such as SAV2 nsP2, a uGDT of >50 is a good indicator. The structural model contains a predicted N-terminal helicase domain (amino acids [aa] 1 to 470) based on homology modeling of the chikungunya (CHIKV) nsP2 helicase domain template (PDB identifier [ID] 6JIM; $P = 1.02 \times 10^{-12}$) and a C-terminal protease domain (aa 471 to 857) based on the CHIKV nsP2 protease domain template (PDB ID 3TRK; $P = 8.38 \times 10^{-6}$). SAV2 nsP2 subdomains in the helicase (N domain, aa 1 to 181, in brown; helicase, aa 182 to 468, in red) and protease (protease, aa 469 to 625, in yellow; C domain, aa 626 to 857, in green) domains were defined based on amino acid sequence alignment with the CHIKV nsP2 protein sequence (Fig. 4B). Furthermore, the SAV2 nsP2 protein sequence was submitted to the cNLS Mapper server to predict putative nuclear localization signals (NLS) (39). This analysis revealed the presence of a

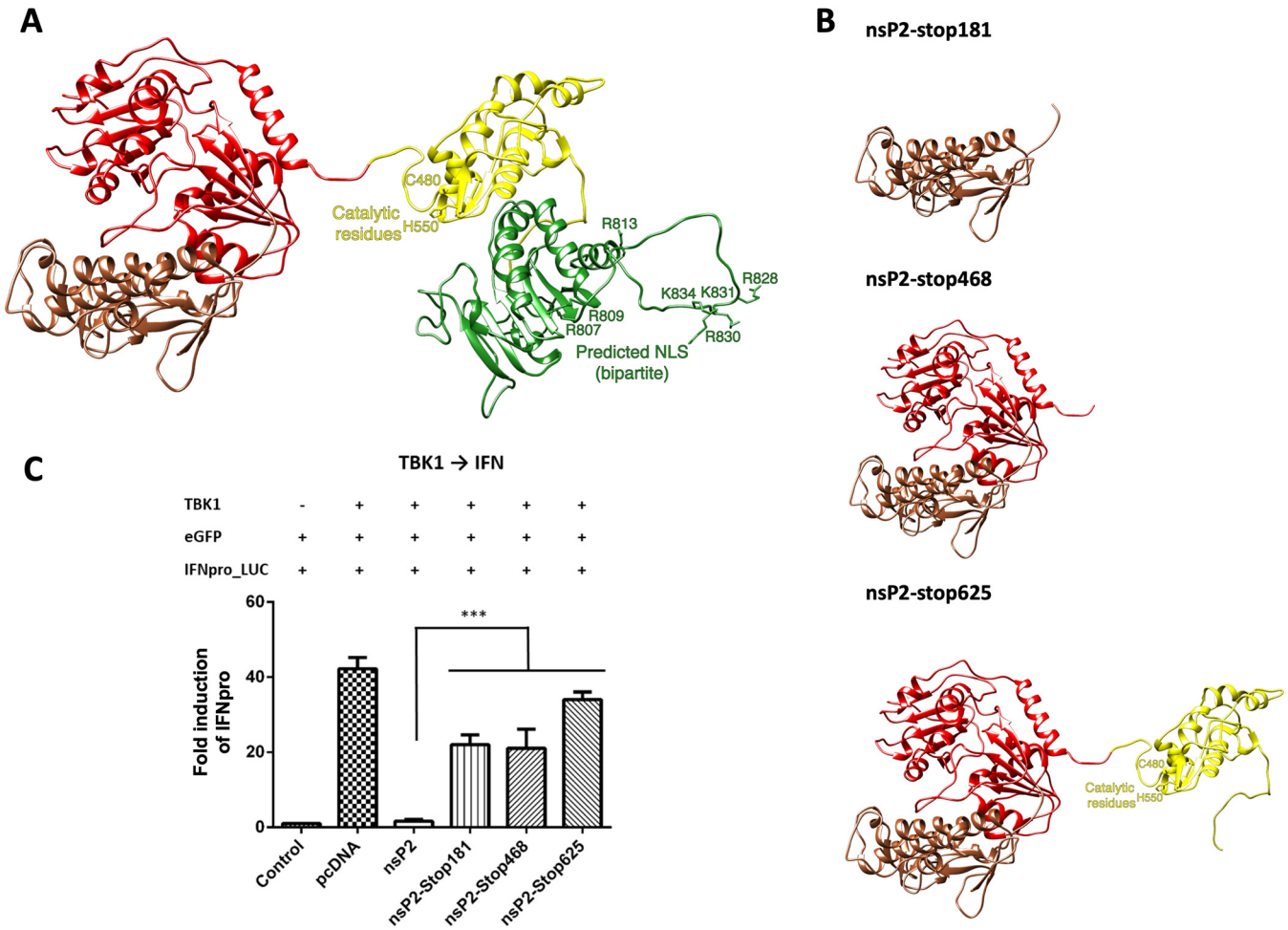

FIG 4 The nsP2 C-terminal domain is required for blocking IFN1 promoter activation. (A) Model of SAV2 nsP2 protein structure. The catalytic dyad of the nsP2 protease domain, consisting of residues C480 and H550, and the putative bipartite NLS composed of residues R807, R809, and R813 (cluster 1, NLS1) and R828, R830, K831, and K834 (cluster 2, NLS2) are shown. (B) SAV2 nsP2 deletion mutant predictive structures generated by insertion of a premature stop codon in the nsP2 gene. Successive deletion of each individual domain of the nsP2 protein has been performed from the C terminus to the N terminus. (C) EPC cells were transfected with the nsP2 deletion mutant constructs (1 μg) together with the IFN1 promoter luciferase reporter plasmid (1 μg) and TBK1 as inducers (1 μg). At 48 after transfection and incubation at 14°C, the cells were lysed for luciferase assays. Luciferase activity was measured and normalized to eGFP fluorescence. Fold inductions were calculated as the ratio of stimulated (+TBK1) versus unstimulated (control; −TBK1) samples. Averages of at least three independent experiments are shown together with standard errors. Groups that are significantly different are denoted by *** ($P < 0.001$).

putative bipartite NLS located in the C domain of the SAV2 nsP2 protease domain (aa 806 to 835). For a given query protein sequence, the cNLS Mapper server calculates an NLS score (range, 1 to 10), with a higher score indicating stronger NLS activity. In the case of SAV2 nsP2, the predicted bipartite NLS has a score of 6.6, which corresponds to a predicted partial localization of the protein to the nucleus, a prediction that is in agreement with the immunofluorescence analysis performed in nsP2-expressing cells (Fig. 3).

The C-terminal domain of nsP2 is essential and sufficient to block RIG-I-mediated interferon expression. To define the minimal domain involved in the inhibition of IFN induction, premature stop codons were introduced in the nsP2 gene in order to successively remove each domain from the C terminus to the N terminus, based on the model structure of nsP2 (Fig. 4A). Three deletion mutants were generated, named nsP2-stop181, nsP2-stop468, and nsP2-stop625 and corresponding to the N-terminal domain alone, the N-terminal and the helicase domains, or the N-terminal, the helicase, and the protease domains, respectively (Fig. 4B). As shown in Fig. 4C, the three deletion mutants of nsP2 lose their ability to inhibit TBK1-mediated induction of IFN1 promoter compared to the full-length form of nsP2. Because the three deletion mutants

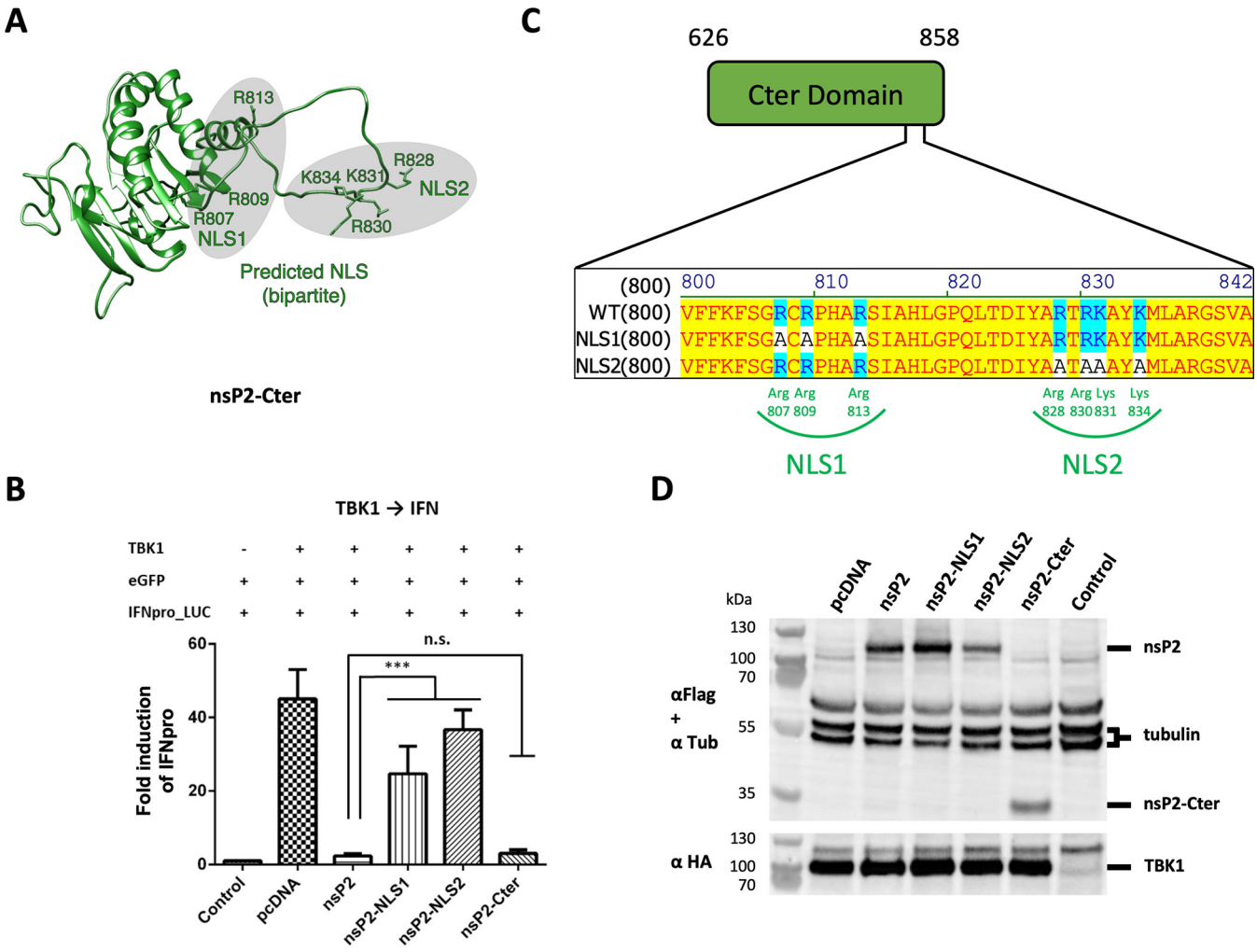

FIG 5 The nsP2 C-terminal domain is sufficient to block IFN1 promoter activation and is dependent on the presence of a putative bipartite NLS. (A) Prediction of the C-terminal domain structure of the SAV2 nsP2 protein. The putative bipartite NLS composed of R807, R809, and R813 (cluster 1, NLS1) and R828, R830, K831, and K834 (cluster 2, NLS2) is shown. (B) EPC cells were transfected with the nsP2 C-terminal domain or with full-length nsP2 NLS mutant constructs (1 μg) together with the IFN1 promoter luciferase reporter plasmid (1 μg) and TBK1 as inducers (1 μg). At 48 h after transfection and incubation at 14°C, the cells were lysed for luciferase assays. Luciferase activity was measured and normalized to eGFP fluorescence. Fold inductions were calculated as the ratio of stimulated (+TBK1) versus unstimulated (control; −TBK1) samples. Averages of at least three independent experiments are shown together with standard errors. Groups that are not significantly different are denoted by "n.s." ($P > 0.05$), whereas those that are significantly different are denoted by *** ($P < 0.001$). (C) Mutagenesis of the bipartite NLS of SAV2 nsP2 protein. Arginine and lysine residues were mutated to alanine residues, leading to two nsP2 mutants lacking one or the other cluster of the bipartite NLS, named NLS1 and NLS2, respectively. (D) EPC cells were transfected with 1 μg of empty plasmid (pcDNA) or 1 μg of a plasmid carrying genes for 3×Flag-nsP2 proteins and a plasmid carrying genes TBK1 fused to a hemagglutinin (HA) tag. Cells were lysed 24 h posttransfection, and equal amounts of proteins were separated by SDS-PAGE. The expression of nsP2 proteins was detected by using an anti-Flag antibody, HA-TBK1 was detected using an anti-HA antibody, and alpha-tubulin expression levels were determined as loading controls.

all lack the C-terminal domain of nsP2, this particular domain (aa 626 to 858; Fig. 5A) was tested for its antagonistic activity on IFN1 promoter induction. As shown in Fig. 5B, the C-terminal domain alone was as efficient as the full-length nsP2 protein to block the IFN1 promoter induction by overexpression of TBK1.

Nuclear localization signals are essential for nsP2-mediated inhibition of IFN induction. The sequence analysis of the C-terminal domain of nsP2 highlighted the presence of a bipartite NLS composed of a first cluster of positively charged arginine (R) residues at positions 807, 809, and 813 (NLS1) and a second cluster of R residues at positions 828 and 830 and lysine (K) residues at positions 831 and 834 (NLS2) (Fig. 5A and C). Each NLS cluster (NLS1 and NLS2) was independently mutated by site-directed mutagenesis within the full-length form of nsP2, leading to nsP2-NLS1 and nsP2-NLS2, respectively (Fig. 5C). As shown in Fig. 5B, both NLS mutants of nsP2 lose their ability

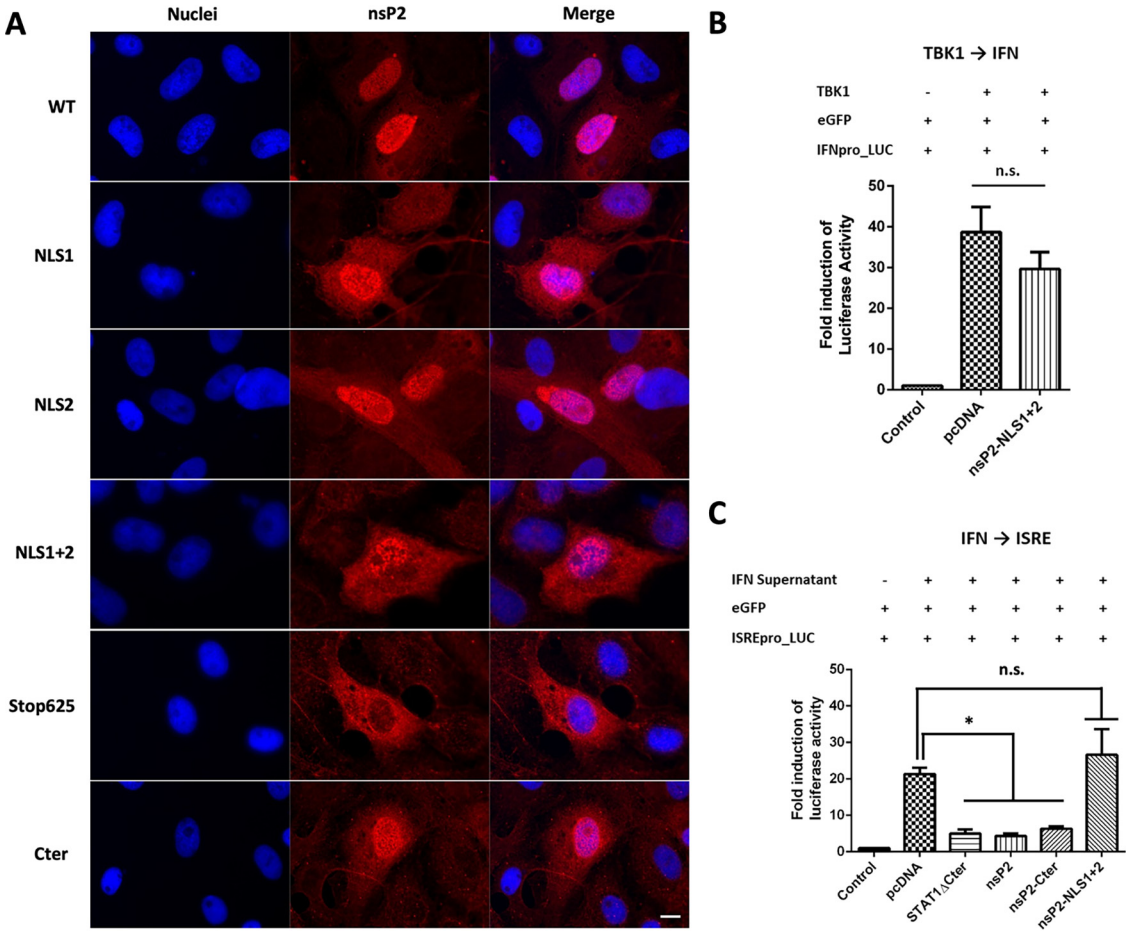

FIG 6 Localization of nsP2 mutants in EPC cells. (A) EPC cells were transfected with 0.5 μg of expression vector encoding nsP2 mutants fused to a 3×Flag tag, incubated for 48 h at 14°C, and then fixed. nsP2 mutant proteins were detected using an anti-Flag MAb (red). Nuclear DNA was stained with DAPI (blue). Bars, 10 μm. (B) EPC cells were transfected with the nsP2 NLS1+2 construct (1 μg) together with the IFN1 promoter luciferase reporter plasmid (1 μg) and TBK1 as inducers (1 μg). At 48 h after transfection, luciferase activity was measured and normalized to eGFP fluorescence. Fold inductions were calculated as the ratio of stimulated (+TBK1) versus unstimulated (control; −TBK1) samples. Averages of three independent experiments are shown together with standard errors. Groups that are not significantly different are denoted "n.s." ($P > 0.05$). (C) EPC cells were transfected with the indicated plasmids (1 μg) together with luciferase reporter constructs (1 μg) driven by an ISRE promoter, and stimulated by IFN1-containing supernatant. Forty-eight hours after transfection and incubation at 20°C, the cells were lysed for luciferase assays. Luciferase activity was measured and normalized to eGFP fluorescence expressed from a peGFP plasmid. Fold inductions were calculated as the ratio of stimulated (+IFN1) versus unstimulated (control; −IFN1) samples. Averages of three independent experiments are shown together with standard errors. Groups that are not significantly different from the pcDNA control condition are denoted by "n.s." ($P > 0.05$), whereas those that are significantly different are denoted by * ($P < 0.05$).

to inhibit TBK1-mediated induction of IFN1 promoter compared to the wild-type (wt) nsP2 protein and the nsP2 C-terminal domain. Western blot analysis confirmed that all forms of nsP2 were expressed in transfected fish cells. Similar amounts of TBK1 were also detected, regardless of which nsP2 variant was coexpressed or compared to the empty vector control (Fig. 5D). To confirm the effect of each NLS cluster mutation on nsP2, we studied the subcellular localization of nsP2 mutants by indirect immunofluorescence assay in EPC cells. As previously observed, wt nsP2 was mainly found in the nucleus of transfected cells (Fig. 6A). Similarly, the C-terminal domain of nsP2, nsP2 Cter, accumulates in the nucleus. In contrast, although still present in the nucleus, both NLS mutants were abundantly found in the cytoplasm of transfected cells. Similarly, a mutant in which both NLS were abolished, nsP2 NLS1+2, was distributed in both subcellular compartments, although it completely lost its ability to block both IFN and ISG induction (Fig. 6B and C). Finally, the C-terminal deletion mutant of nsP2, nsP2-

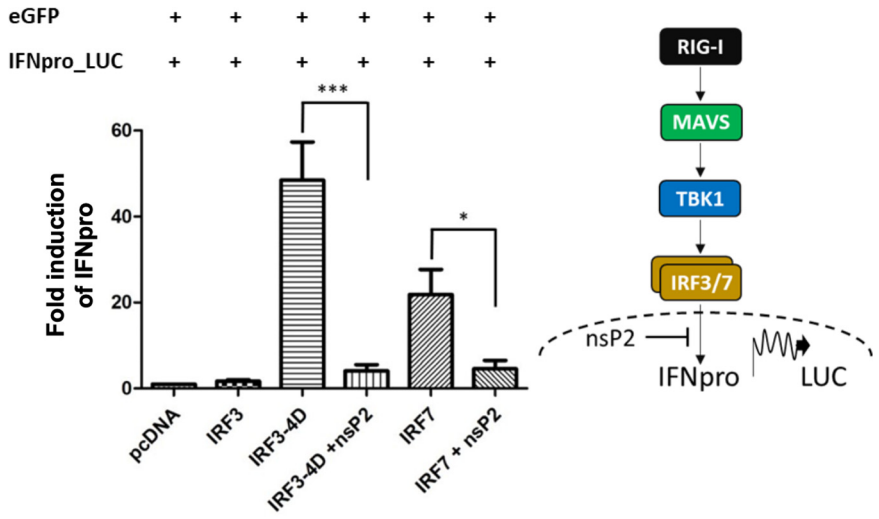

FIG 7 nsP2 blocks the induction of IFN expression mediated by IRF3/7. EPC cells were transfected with the nsP2-encoding plasmid (1 μg) together with the IFN1 promoter luciferase reporter plasmid (1 μg) and IRF3-4D or IRF7 as inducers (1 μg). At 48 h after transfection and incubation at 20°C, the cells were lysed for luciferase assays. Luciferase activity was measured and normalized to eGFP fluorescence. Fold inductions were calculated as the ratio of stimulated (+IRF3/7) versus unstimulated (control; −IRF3/7) samples. Averages of at least three independent experiments are shown together with standard errors. Groups that are significantly different are denoted by * ($P < 0.05$) or *** ($P < 0.001$). Schematic representation of the RIG-I pathway leading to the induction of type-I interferon and model of nsP2 inhibitory mode of action. nsP2 translocates into the nucleus and blocks IFN promoter activation by activated forms of transcriptional factors IRF3/7.

Stop625, was exclusively found in the cytoplasm. These results suggest that the determinants for the antagonist function of nsP2 against cellular antiviral signaling (IFN and ISG responses) are found in the 232 C-terminal amino acids together with the elements driving the nuclear translocation of nsP2.

nsP2 inhibits IFN induction downstream of IRF3. To determine precisely at which level within the pathway nsP2 blocks RIG-I signaling, we tested its blocking activity using our cell-based luciferase reporter system induced by IRF3-4D. IRF3-4D is a constitutively active form of IRF3 that does not need to be phosphorylated to enter the nucleus and activate the IFN promoter. The expression of IFN mediated by IRF3-4D was blocked in the presence of nsP2 (Fig. 7). The same result was observed when the pathway was induced by IRF7. To check whether nsP2 interacts directly with IRF3, we cotransfected nsP2 and IRF3-4D in EPC cells. Immunofluorescence analysis showed that IRF3-4D and nsP2 were not localized in the same subcellular compartment, suggesting that they are not likely to be interacting (Fig. 8A). This result was confirmed by coimmunoprecipitation assays (Fig. 8B), where no interaction between IRF3-4D and nsP2 were found. These findings suggest that the IFN blockade mediated by nsP2 occurs at a stage downstream of IRF3, and not by directly targeting transcription factors.

Because IRF3-4D was unexpectedly not found in large amounts in the nucleus when transfected alone in EPC cells, we wanted to confirm whether IRF3-4D was still able to effectively induce IFN in fish cells. EPC cells were transfected with IRF3 or IRF3-4D plasmids and were infected at 72 h posttransfection with a recombinant fish rhabdovirus expressing the Tomato reporter gene, rVHSV-Tomato, at a multiplicity of infection (MOI) of 1 and incubated at 15°C. Viral hemorrhagic septicemia virus (VHSV) is a virulent virus that efficiently and rapidly infects EPC cells. As such, it is a good model to test for cellular protection against viral infections. At 48 h postinfection, supernatants were collected and titers were determined. IRF3-4D efficiently protected EPC cells against rVHSV-Tomato (Fig. 8C), while IRF3 did not. Titer determination of supernatants showed a 2-log decrease between IRF3 and IRF3-4D conditions, confirming that despite not being exclusively detected in nuclei, IRF3-4D retains its activity.

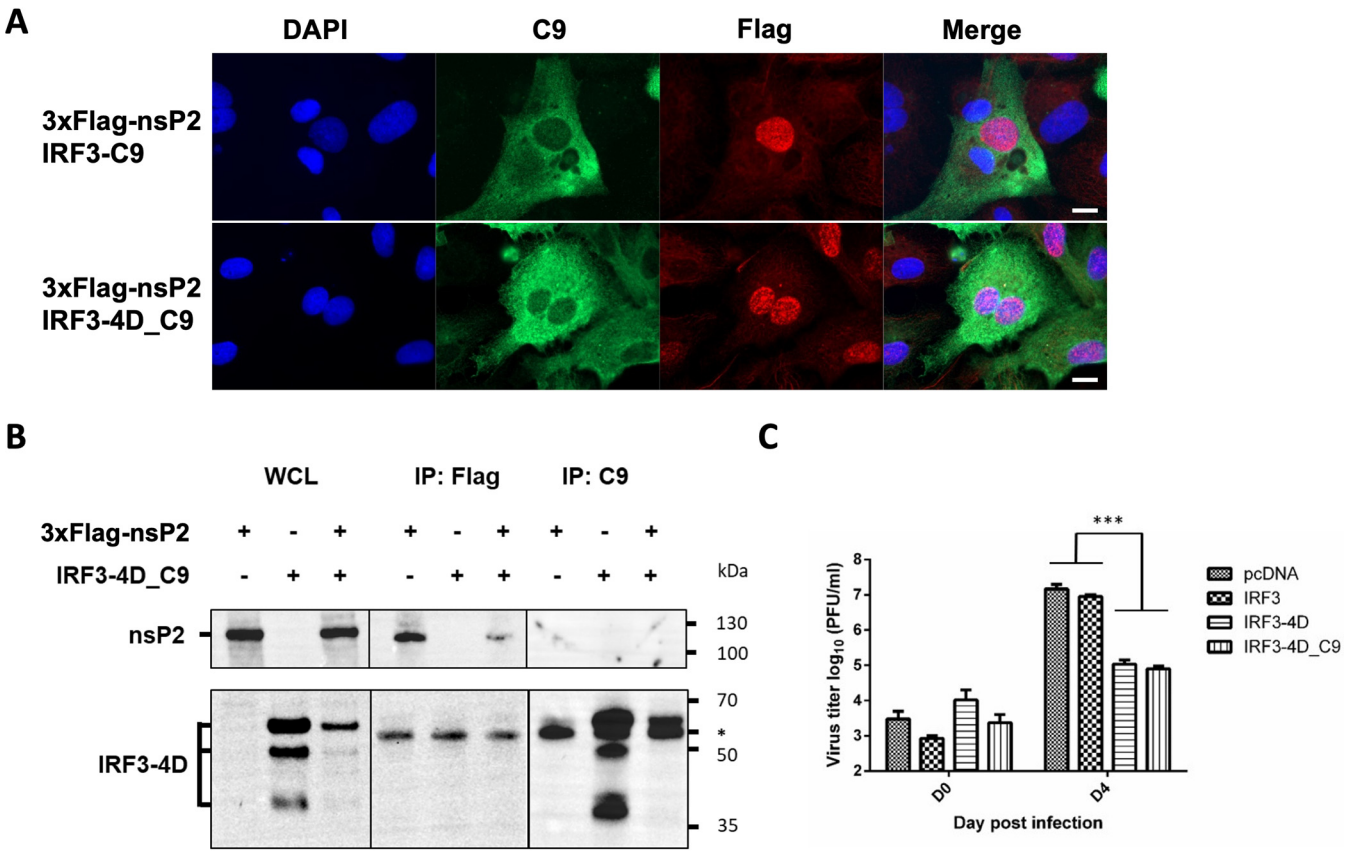

FIG 8 nsP2 does not interact with IRF3. (A) EPC cells were transfected with 1 μg of an expression vector encoding nsP2 fused with a 3×Flag epitope tag and/or IRF3/IRF3-4D fused with a C9 epitope tag. Cells were incubated for 48 h at 14°C and then fixed. nsP2 protein was detected using an anti-Flag MAb (red), and IRF3/IRF3-4D were detected using anti-C9 MAb (green). Nuclear DNA was stained with DAPI (blue). Bars, 10 μm. (B) Epitope-tagged nsP2 and IRF3-4D proteins do not interact with each other in EPC cells. Cells were cotransfected with 2 μg of the indicated plasmids. At 72 h posttransfection, the lysates were immunoprecipitated (IP) with anti-Flag or anti-C9 as indicated, followed by immunoblotting (IB) analysis with anti-Flag or anti-C9. "WCL" corresponds to the expression of exogenous proteins in whole-cell lysates. An asterisk (*) corresponds to the detection of heavy chains of mouse or rabbit immunoglobulins used for IP. (C) EPC cells were transfected with IRF3 or IRF3-4D with or without C9 epitope tag (2 μg). At 72 h posttransfection, cells were infected with rVHSV-Tomato and incubated at 14°C. Supernatants were collected at 0 and 4 days postinfection. Virus titers were determined by plaque assay. Error bars represent standard deviation of duplicates. Groups that are significantly different are denoted by *** ($P < 0.001$).

SAV2 strains with NLS-modified nsP2 are strongly attenuated. To test whether nsP2 nuclear localization is critical for SAV2 replication, we used a pSAV2 construct, which possess the full-length SAV2 genomic sequence under the control of a cytomegalovirus (CMV) promoter allowing recovery of recombinant viruses (40). Each nsP2 NLS cluster previously described was independently or jointly mutated by site-directed mutagenesis. Mutated constructs were used to transfect susceptible BF-2 cells for recovery of 3 rSAV2 recombinants, rSAV2.ΔNLS1, rSAV2.ΔNLS2, and rSAV2.ΔNLS1+2 (Fig. 9A). rSAV2 mutant viruses could not be recovered for rSAV2.ΔNLS1 and rSAV2.ΔNLS1+2 after one passage on BF-2 cells in three independent transfection assays (Fig. 9B). However, rSAV2.ΔNLS2 could be recovered, but was strongly attenuated compared to rSAV2wt (Fig. 9B). rSAV2.ΔNLS2 was amplified on BF-2 cells after three consecutive passages. rSAV2.ΔNLS2 stock reached a titer of 2×10^7 PFU/ml, which is similar to that of the wild-type virus. The entire nsP2 open reading frame (ORF) was sequenced, and no additional mutations were observed except those introduced in the NLS2 sequence. Both rSAV2.WT and rSAV2.ΔNLS2 viruses were then compared for their kinetics of replication in BF-2 cells; the multistep growth curve is shown in Fig. 9C. BF-2 cells were infected at an MOI of 0.1. rSAV2.ΔNLS2 is significantly attenuated compared to the wild-type virus, with a slower kinetics of viral production and an almost 10-fold decrease in the final titer at day 14 postinfection. Finally, CHSE-214 salmonid cells were

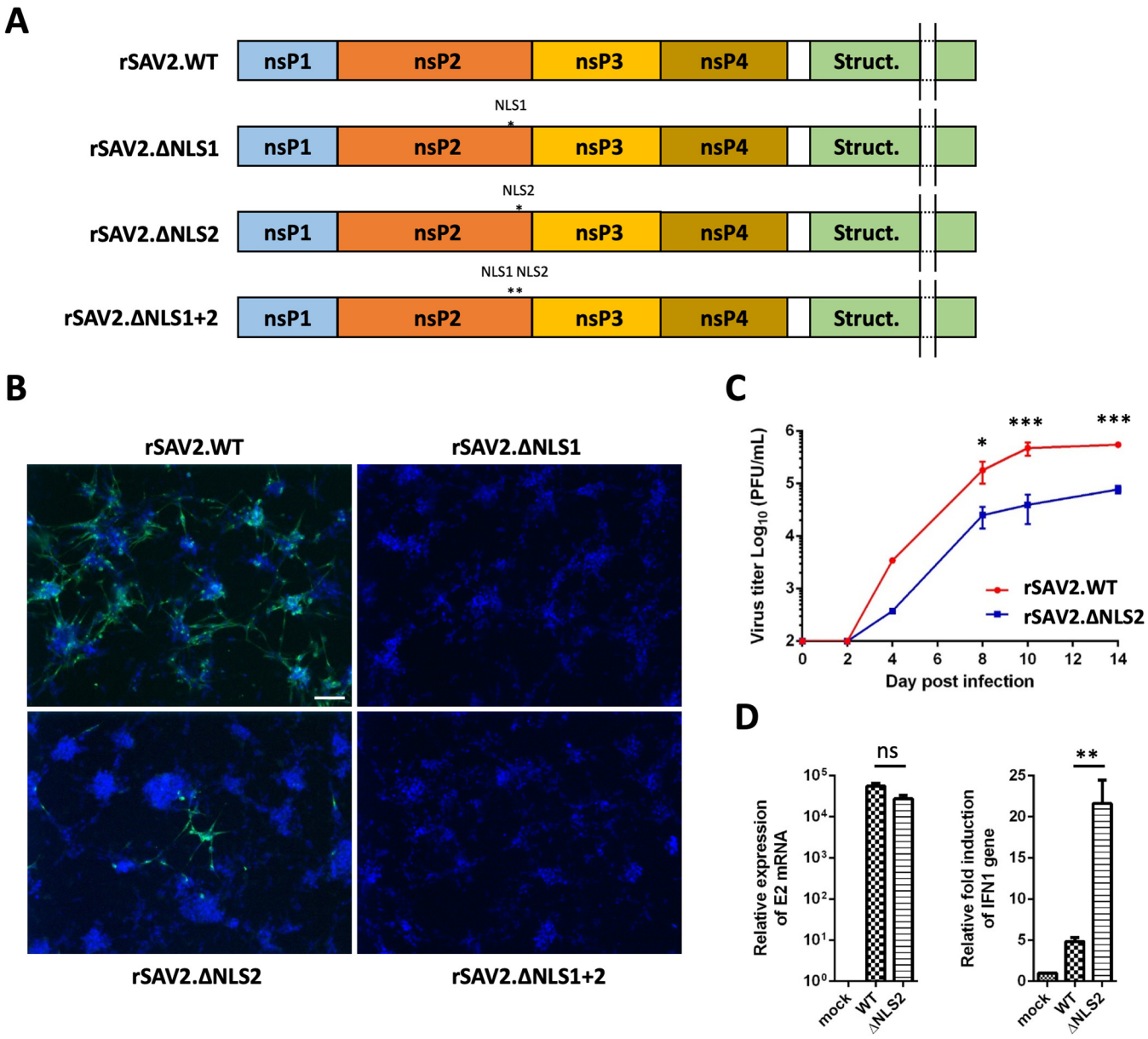

FIG 9 Recombinant SAV2 NLS mutants are strongly attenuated *in vitro*. (A) Schematic representation of wild-type SAV2 and SAV2 mutants with modified NLS clusters. (B) BF-2 cells were transfected with 2 μg of pSAV2 constructs. Supernatants were collected at 14 days posttransfection, and recovered viruses were used to infect BF-2 cells. The cells were fixed after 12 days. Infected cells were labeled using an anti-E2 MAb (green). Nuclear DNA was stained with DAPI (blue). (C) BF-2 cells were infected with rSAV2.ΔNLS2 or SAV2.WT at a multiplicity of infection (MOI) of 0.1. At the indicated times postinfection, cell supernatant was collected and the virus titer was determined. Each time point was represented by two wells, and each virus titer was determined in duplicate. Means are shown, and the standard errors were calculated. Virus titers that are significantly different are denoted by * ($P < 0.05$) and *** ($P < 0.001$). (D) CHSE-214 cells were infected at an MOI of 1 PFU per cell with wild-type rSAV2 or rSAV2.ΔNLS2 were or mock-infected. At 96 h postinfection, total RNA was extracted and reverse transcription performed. Quantitative real-time PCR was conducted using primers targeting E2 and IFN1. The EF1A gene was used as an internal control to normalize the cDNA template and for real-time PCR calculations. The standard deviations for triplicate experiments are shown. Asterisks (**) indicate significant difference ($P < 0.01$); n.s., not significant ($P > 0.05$).

infected at an MOI of 1 with rSAV2.WT or rSAV2.ΔNLS2 or were mock-infected. At 96 h postinfection, viral replication and IFN1 expression were analyzed by reverse transcription-quantitative PCR (RT-qPCR). As shown in Fig. 9D, E2 mRNA expression was similar for both viruses. In contrast, IFN1 expression was highly induced in rSAV2.ΔNLS2-infected cells compared to that in those infected with the wild-type virus. Despite not being able to recover all recombinant viruses, our findings confirm that nsP2 localization in the nucleus is important for inhibiting the IFN pathway and allowing SAV2 to replicate efficiently in fish cells.

DISCUSSION

Arboviruses have developed strategies to directly or indirectly interfere with type I IFN signaling, often thanks to their nonstructural proteins. Among them, terrestrial alphaviruses are especially sensitive to type I IFNs (41–44), and therefore have evolved countermeasures. Here, we report that SAV2, a marine alphavirus, efficiently blocks both RIG-I signaling and IFN response in fish cells via its nsP2 and, to a lesser extent, via nsP3. This is a potential cooperative inhibition effect of both nsP2 and nsP3 proteins on RIG-I signaling. Indeed, during the maturation of the nsP1-2-3-4 polyprotein, nsP2 and nsP3 are cleaved last, after nsP1 and nsP4 are released (45). The nsP2-3 polyprotein is unable to translocate in the nucleus, suggesting that nsP2 blocking occurs later during cell infection (46). Thus, nsP2-3 may be the protein responsible for blocking the RIG-I pathway at the early stage of the infection, together with the amount of mature nsP2 brought by the viral particles (47).

In our reporter system, this blockage is dependent on nsP2 nuclear localization of its C-terminal domain. A similar effect has recently been described for chikungunya virus nsP2, along with its structural proteins E1 and E2, which were found to block the activation of nuclear factor kappa B (NF-κB) signaling (48). Moreover, nsP2 appears to also block ISRE-mediated expression of ISGs. This pathway, controlled by the JAK-STAT signal transduction, has been described to be inhibited by nsP2 encoded by terrestrial alphaviruses. For instance, Venezuelan equine encephalitis virus (VEEV), a New World alphavirus, is able to disrupt STAT1 nuclear localization (49). Similar findings have been reported for Old World alphaviruses, such as chikungunya virus, whose nsP2 can block STAT1 phosphorylation and/or nuclear translocation (50) and can promote its nuclear export (51) in mammalian cells. These results suggest that nsP2 possesses a key role for escaping innate immunity, by targeting both RIG-I and IFN signaling, and that this function appears to be conserved among other alphaviruses.

In terrestrial alphaviruses, nsP2 was found to be responsible for inducing rapid degradation of Rpb1, a catalytic subunit of the RNApol II (52). This degradation, which is independent of nsP2 protease activity, leads to a global cellular transcriptional shutoff. This phenomenon, occurring during infection, prevents transcription of IFN and ISGs (53). Interestingly, the cellular shutoff does not appear to occur during SAV infection. Furthermore, we demonstrated that mutation of the two conserved catalytic residues (Cys 480 and His 550) of nsP2 does not impact its effect on IFN induction. Moreover, the deletion of the entire protease domain in the nsP2 C terminus has no effect on nsP2 inhibitor function. We can conclude that, unlike terrestrial alphaviruses, IFN blockade does not require cellular shutoff during SAV2 infection, but similarly the protease function of nsP2 does not participate in the RIG-I signaling inhibition.

Expression of nsP2 completely prevents induction of type I IFN by the constitutively active form of IRF3 (IRF3-4D). This finding suggests that the blockade of IFN induction by nsP2 occurs downstream of IRF3, a critical transcription factor that activates IFN promoter in the nucleus, and raises the question of where this inhibition takes place. SAV2 nsP2 is predicted to possess two NLS, positioned at the C-terminal extremity of the protein. Our immunofluorescence assays showed that nsP2 is mostly located in the nucleus. Truncated forms of nsP2 that no longer have a C-terminal domain are unable to block type I IFN induction and are no longer detected in the nucleus by immunofluorescence, suggesting that nsP2 localization in the nucleus is controlled by the C-terminal domain of nsP2. Moreover, assays using nsP2 with mutated NLS clusters (Fig. 10A and B) showed that despite keeping a partial localization in the nucleus, the mutants were no longer able to block type I IFN induction. This has already been reported for Sindbis virus nsP2 by Frolov and colleagues (54). Mutations in Sindbis virus nsP2 NLS1 and NLS2 do not abrogate import of this protein into the nucleus, indicating that nsP2 can be transported into the nucleus by mechanism(s) other than those mediated by a standard NLS. However, an additional cryptic NLS is predicted in the C-terminal domain of nsP2 (Fig. 10B) and might be the driving force of nsP2 translocation into the nucleus. In addition, these results also suggest that the NLS may be directly involved in nsP2

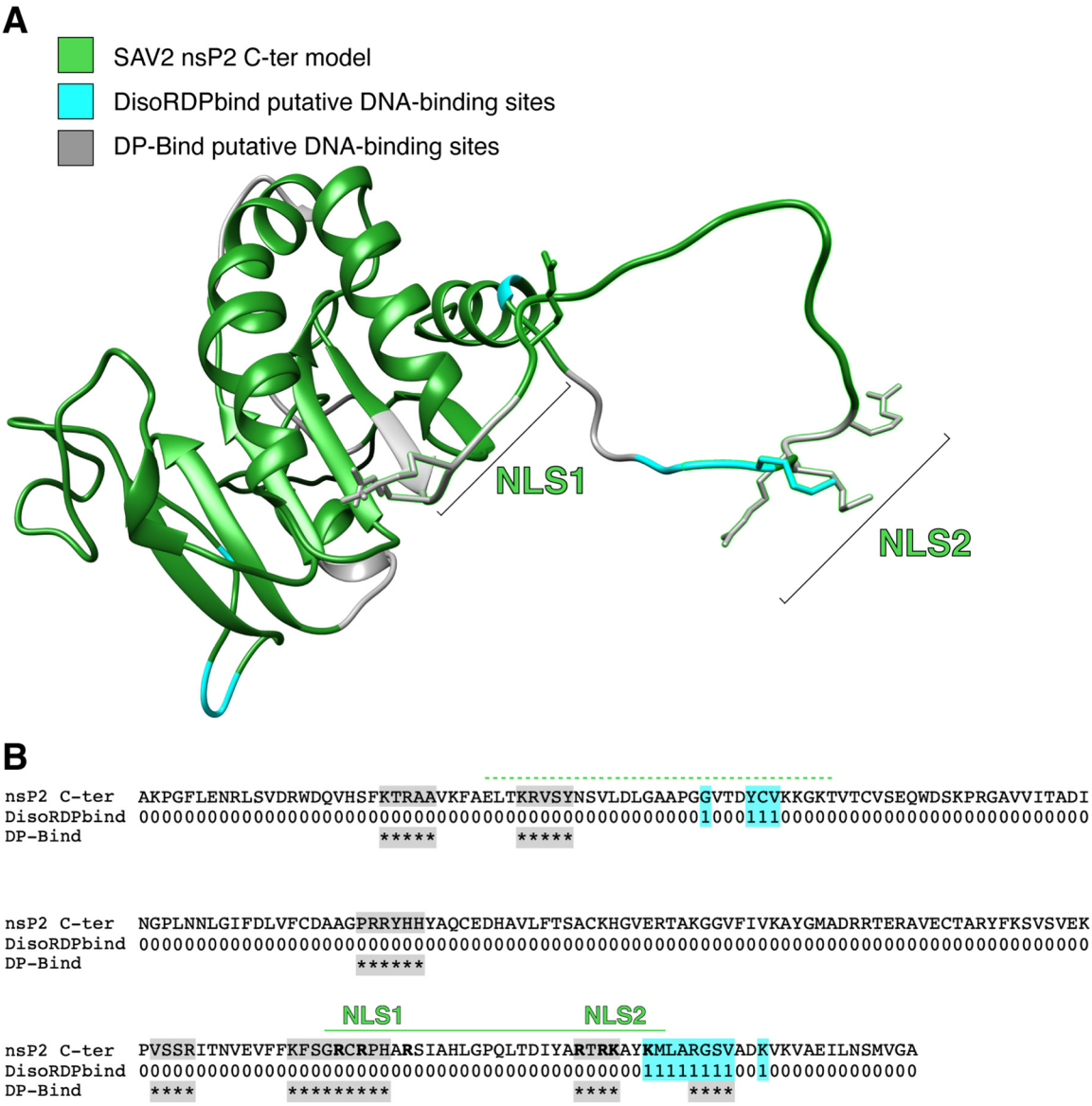

FIG 10 Predicted structure and functional motifs of the SAV2 nsP2 C-terminal methyltransferase-like domain. (A) Structural homology-based model of the SAV2 nsP2 C-terminal domain. Structural modeling was performed using Chimera X. The structural model was visualized and annotated using UCSF Chimera. The putative bipartite NLS predicted by NLS Mapper and composed of R807, R809, and R813 (cluster 1, NLS1) and R828, R830, K831, and K834 (cluster 2, NLS2) is shown together with the putative DNA binding domains identified by DisoRDPbind and DP-Bind analyses. For the latter, stretches of four or more residues predicted to bind DNA are shown. (B) Mapping of NLS and DNA binding sequences. The amino acid composition of the C-terminal domain of nsP2 (residues 624 to 857) is displayed along with putative DNA binding sites located in intrinsically disordered regions (DisoRDPbind; "1" corresponds to a residue predicted to be involved in DNA binding) and putative NLS. The solid green line corresponds to the bipartite NLS identified using NLS Mapper with a score of 6.6, with NLS1 and NLS2 basic residue clusters (in bold) shown. The dashed green line corresponds to a possible cryptic NLS (low score of 2.7). Additional DNA binding motifs were identified using the DP-Bind server (asterisks [*] correspond to stretches of more than 4 residues predicted to participate in DNA binding). Partial overlapping of predicted NLS and DNA binding regions is observed for both NLS-1 and NLS-2.

inhibitory function against type I IFN induction in the nucleus. These conclusions are supported by the fact that viruses carrying mutated NLS are extremely attenuated, to the point that it is difficult to recover them *in vitro*. Interestingly, only rSAV2.ΔNLS2 has been recovered and amplified in BF-2 cells, showing reduced replication fitness and a higher induction of IFN1 in salmonid cells compared to those of the wild-type virus. This is in line with another study, which showed that a mutant Semliki Forest virus (SFV) with a single mutation in the NLS within nsP2 induced significantly more IFN

than wt SFV, despite similar replication levels (55). The authors suggest that nuclear entry of nsP2 has clear effects on cellular innate immune signaling genes, similar to what we observed with SAV2 nsP2.

Interestingly, our results showed that nsP2 does not appear to interact with IRF3. The punctiform staining observed for nsP2 in the nucleus suggests that nsP2 may be able to recognize specific DNA sequences found in the host genome. Such putative binding at specific DNA regions may be responsible for the observed IFN inhibition, for example by targeting promoters of specific genes. Similar effects have been described for other viruses, such as Kaposi's sarcoma-associated virus (KSHV). KSHV leucine zipper-containing transcription factor (K-bZIP) and latency-associated nuclear antigen (LANA-1) protein are able to bind to the IFN-β promoter, preventing IRF3 binding and subsequent IFN-β transcription (56, 57). Human cytomegalovirus (HCMV) protein UL44 has also been described as inhibiting IRF3 binding on promoter regions of downstream antiviral genes (58). Interestingly, the C-terminal domain of nsP2 (232 amino acids), which still possess the two NLS, was able to block IFN induction as efficiently as full-length nsP2. This result was particularly surprising, since the C-terminal domain does not have nsP2 helicase function, located in the N-terminal part of the full-length protein, which would have been a good candidate for binding to DNA. Similarly, the C-terminal methyltransferase-like (MTase) domain of chikungunya virus nsP2 is sufficient to induce nuclear export of phosphorylated STAT1 when artificially addressed to the nucleus by an unknown mechanism that does not require the helicase activity of nsP2 (51). The authors suggested that nsP2 C-terminal domain recruits a cellular DNA binding protein involved in transcriptional regulation to compete with STAT1 binding to ISRE promoters. Protein sequence-based analyses of the nsP2 C-terminal domain using two complementary DNA binding prediction tools, DisoRDPbind and DP-Bind (59, 60), suggest that DNA binding sites are present in the SAV2 nsP2 C-terminal domain, with some sites predicted to overlap the bipartite NLS sequence (Fig. 10A and B). Thus, mutation of these NLS sequences might impact their putative DNA binding activity, which could account for our observation of the loss of activity of nsP2 despite it still being present in the nucleus. This supports the hypothesis of a competition of nsP2 with host transcription factors for enhancer sequences in specific promoters and the dual functions of the intrinsically disordered C-terminal region involved in both nuclear localization and blocking of IFN and ISG expression. Of all promoters known to be induced by type I IFN, the ISRE possesses a consensus nucleotide sequence, $GAAAN_{(1\text{-}2)}GAAA$, which is highly conserved among vertebrates, with human ISRE promoters being functionally active in fish cells (61, 62). In salmonids and cyprinids, the ISRE motif exactly matches the IRF-binding element (IRFE) nucleotide sequence, $GAAAN_{(2)}GAAA$, which is present in almost all characterized promoters of type I IFN (63, 64). Hence, these common sequence elements in the regulatory region of virus-inducible promoters make them ideal targets to simultaneously inhibit both IFN and ISG expression.

The predicted structure of the nsP2 C-terminal domain (Fig. 10A) has high structure homology with the MTase domain from flavivirus NS5 protein (100% confidence in Phyre2). Flavivirus NS5 is responsible for replicating and capping the viral genome, but is also a potent innate immune antagonist with a similar nuclear localization to that observed for SAV nsP2 (65). NS5 protein blocks not only the antiviral response by antagonizing RLR signaling, but also STAT transcription factors that are involved in interferon-α/β receptor (IFNAR) signaling. As an example, dengue virus (DENV) NS5 binds human STAT2 and targets it for ubiquitin-mediated proteasomal degradation. The MTase domain of NS5 is required for the repression of RIG-I, and NS5 is able to transcriptionally regulate specific genes within the nucleus. Nuclear localization of NS5 is essential for DENV replication (66). DENV NS5 interacts with and antagonizes polymerase-associated factor 1 complex (PAF1C) (67). This nuclear complex promotes the expression of many genes, including genes related to the antiviral, antimicrobial, and inflammatory responses. Flavivirus NS5 antagonizes PAF1C by inhibiting its recruitment to immune response genes, similarly to influenza A virus NS1 protein (68). Both NS5

and NS1 proteins selectively affect inducible gene expression, thus contributing to suppression of the antiviral response.

While our study clearly demonstrates the crucial role played by SAV2 nsP2 in inhibiting RIG-I-mediated IFN responses, more detailed analyses will allow a better understanding of the mechanisms by which this virus evades innate immunity. This will not only shed light on how an aquatic alphavirus escapes innate sensing and thus evades the innate immune system of its fish host, but will also inform on how these host evasion strategies have evolved in both aquatic and terrestrial members of the genus *Alphavirus*.

MATERIALS AND METHODS

Cells and virus. EPC cells (epithelioma papulosum cyprini from fathead minnow, *Pimephales promelas*), CHSE-214 cells (Chinook salmon, *Oncorhynchus tshawytscha*), and BF-2 cells (Bluegill fry, *Lepomis macrochirus*) were maintained in Glasgow's modified Eagle's medium (GMEM) containing 25 mM 4-(2-hydroxyethyl)-1-piperazineethanesulfonic acid (HEPES; Eurobio) supplemented with 10% fetal bovine serum (FBS; Eurobio), 1% tryptose phosphate broth (Sigma), 2 mM L-glutamine (PAA), and penicillin (100 U/ml)-streptomycin (100 μg/ml) (BioValley) and incubated at 24°C for EPC cells and at 20°C for CHSE-214 and BF-2 cells. Recombinant SAV (rSAV) was propagated in monolayer cultures of BF-2 cells in serum-free GMEM-HEPES at 10°C. At 12 days postinfection, virus detection was performed by indirect immunofluorescence assays. Infected BF-2 cells were fixed with a mixture of ethanol and acetone (1:1 [vol/vol]) at −20°C for 15 min and then air dried. Fixed BF-2 cells were incubated for 45 min at room temperature with primary mouse monoclonal antibody (MAb) clone 17H23 against SAV E2 protein (9, 69) diluted at 1:10,000 in phosphate-buffered saline (PBS) containing 0.05% Tween 20 (PBS-T), and washed three times in PBS-T. The cells were then incubated for 45 min at room temperature with Alexa Fluor 488-conjugated anti-mouse antibody (Invitrogen) diluted at 1:2,000 in PBS-T and then washed three times in PBS-T. Cell monolayers were then visualized directly with a UV-light microscope (Carl Zeiss) after mounting of the coverslips using ProLong Gold antifade reagent with 4′,6-diamidino-2-phenylindole (DAPI) medium (Invitrogen). Recombinant viral hemorrhagic septicemia virus expressing tomato red fluorescent protein (rVHSV-Tomato) was propagated in EPC cells at 15°C as previously described (70). After 1 h of adsorption, the inoculum was removed, the cell monolayer was washed twice, and medium samples (0.2 ml of the 2-ml overlay) were taken (D0 time point) and replaced by an equivalent volume of fresh medium. At 4 days postinfection, supernatant aliquots were harvested; these were analyzed later by plaque assay (71).

Plasmid constructs. An SAV2 sequence (GenBank accession number AJ316246.1 [4]) was used to design primers (Table 1) to amplify either nsP1, nsP2, nsP3, and nsP4 coding sequences or the C-terminal domain of nsP2 (nsP2 Cter) from the infectious cDNA clone pSAV2, previously called pSDV (40). PCR products were purified with a QIAquick PCR purification kit (Qiagen) and cloned into the eukaryotic expression vector pcDNA1.1/Amp (Invitrogen) or into modified versions of pcDNA1.1/Amp adding either an N-terminal triple Flag tag (3×Flag) or an N-terminal hemagglutinin (HA) tag in frame and in fusion with the protein coding sequence. The nsP2 construct was further modified by site-directed mutagenesis using a QuikChange site-directed mutagenesis kit (Stratagene) according to the manufacturer's recommendations in order to mutate the catalytic residues of the nsP2 protease domain or remove nuclear localization signals (NLS) using specific primers (Table 1). Site-directed mutagenesis was also performed to introduce premature stop codons in the nsP2 gene in order to obtain successively truncated versions of the protein lacking different functional domains (primers are listed in Table 1).

Fathead minnow EPC cell line-derived IRF3, IRF7, and STAT1 sequences were identified in expressed sequence tag (EST) libraries from fathead minnow (*Pimephales promelas*) using zebrafish orthologs. Total RNA from EPC cells was extracted using an RNeasy kit (Qiagen) according to the manufacturer's instructions. The RNA was used to generate full-length cDNAs using the Smart rapid amplification of cDNA ends (RACE) cDNA amplification kit (TaKaRa Clontech) with universal primers provided by the manufacturer and gene-specific primers (Table 1) designed from the EST sequences. PCR amplifications were performed using the Advantage 2 PCR kit (TaKaRa Clontech) and following the manufacturer's instructions. RT-PCR products were purified with the QIAquick PCR purification kit (Qiagen), cloned into the pcDNA1.1/Amp vector, and fully sequenced (GenBank accession numbers MN781134, MN781135, and MN781136, respectively). EPC IRF3 was further modified by site-directed mutagenesis in order to replace all serine residues at positions 431, 432, 435, and 441 by aspartic acid residues, which mimic phosphorylation, leading to a constitutively active form of IRF3 called IRF3-4D. Both forms of IRF3 were finally cloned and fused to a C9 (bovine rhodopsin C terminus) epitope tag at the 5′ end of their coding sequences.

Plasmids encoding the RIG-I N terminus fused to GFP (RIG-I Nter-eGFP), A20, TBK1, and HA-TBK1 from fathead minnow were previously described, as well as the pIFNpro-LUC and pISREpro-LUC plasmids containing the luciferase reporter gene (LUC) under the transcriptional control of the interferon promoter from EPC cells and the interferon-sensitive response element, respectively (30, 61, 72).

Transfection, fluorescence microscopy, and luciferase activity assay. EPC cells were plated into 6-well plates at a density of 5×10^6 cells per well 24 h prior to transfection by electroporation (Amaxa Biosystems, Lonza). Cells were trypsinized and resuspended in 100 μl of electroporation solution T.

TABLE 1 Primers used to construct expression plasmids and pSAV mutants and for qPCR analyses

Primer	Sequence (5′ to 3′)[a]	Restriction site
5nsP1 EcoRI	CCCGAATTCATGATGCAAAATCTCACAGC	EcoRI
3nsP1 XhoI	GGGCTCGAGTTAAGAACCCACCCCGTCTTCTTC	XhoI
5nsP2 EcoRI	CCCGAATTCATGACCATCATTGACTGCCAAAG	EcoRI
3nsP2 XhoI	GGGCTCGAGTTAGGCTCCTACCATCGAGTTGAG	XhoI
5nsP3 EcoRI	CCCGAATTCATGGCGCCGGGCTACAGAGTCCTC	EcoRI
3nsP3 SalI	CCCGTCGACTTACCCTCCGGGGCCGTCACGTTG	SalI
5nsP4 EcoRI	CCCGAATTCATGTATATATTCTCTTCTGACCAAGG	EcoRI
3nsP4 XhoI	GGGCTCGAGTTAGGCGTAGAGGGATACGTACTC	XhoI
nsP2_C480A	GCGCACGGGAAGCGTAACACCGCTTGGGCAGTTACAAGCAGCCG	
nsP2_H550A	GTTTCATGCGTCTGGAGAACAGCGCTTGGAGCAATTCCAACAGAGG	
nsP2_STOP181	GGCCGGCTCACACACACGACTAACACACGATTGGCATCTACGGGG	
nsP2_STOP468	GCGGCTCTCAGAGAAGCATGTTAACCACGGATGAACTTCGCGCAC	
nsP2_STOP625	CTTGTGGACACTTCCGCAGCGTGAAAACCAGGTTTTCTGGAAAACAG	
nsP2_NLS1	CGTGGAAGTCTTTTTTAAATTTTCCGGAGCCTGTGCCCCGCATGCTGCTTCCATTG CACACTTGGGCCCTCAACTGACCG	
nsP2_NLS2	CTTGGGCCCTCAACTGACCGACATCTATGCTGCCACGGCGGCGGCGTACGCAAT GCTGGCGAGAGGAAGTGTCGCTGACAAG	
5nsP2Cter_625 EcoRI	CCCGAATTCATGGCCAAACCAGGTTTTCTGGAAAACAGG	EcoRI
5IRF3 EcoRI	CCCCAATTGATGACCCATCCAAAACCGCTCTTCG	MfeRI
3IRF3 XhoI	GGGCTCGAGTCACTTGGTGTCACACAACTCCATC	XhoI
IRF3_4D	GGAGGGTTTGAACACGTTGGCTGTTTCACGTGGGGCGGATGACCTGCAGGATGT GGAGCTACAACTCGATCTGGAGCAAATGATGGAGTTGTGTGACACC	
5IRF7 EcoRI	CCCGAATTCATGCAGAGCACGATGGGCAAACC	EcoRI
3IRF7 EcoRV	CCCGATATCTTAGTCCATTGAAGGCAGACCC	EcoRV
5STAT1Cter MfeI	CCCCAATTGATGACACTCTGGAACCAGCTGCAGC	MfeI
3STAT1Cter XhoI	GGGCTCGAGTTAAGAGCTGGTATAGTAGCGACC	XhoI
5SAV2SpeI	GATTATTGACTAGTTATTAATAGTAATCAATTACGG	SpeI
3SAV2SpeI	CTCCACTAGTGCGCCGAAGGACTGTTCCAGTC	SpeI
RT SAV_E2_F	GCATCAATGCACCATGGTTT	
RT SAV_E2_R	ATAGAGCGCGGACTTCTTCG	
RT_IFN1_F	AATTCCTGTGTATCACCTGCCA	
RT_IFN1_R	CACGCCTGTGCACTGTAGTT	
RT_EF1A.1_F	CCCTGTACTGGATTGCCACA	
RT_EF1A.1_R	CTTCAGGAACTTGGGGGCAT	

[a]Restriction enzyme sites are underlined; mutated nucleotides are shown in bold.

Plasmid DNA was then added to cells, which were then electroporated using the fish cell-optimized program T-020. At 48 h posttransfection, cells were fixed or lysed for further analysis.

For immunofluorescence microscopy, cell monolayers were fixed with a mixture of ethanol and acetone (1:1 [vol/vol]) at −20°C for 15 min. Antigen detection was performed by incubation with mouse anti-Flag M2 antibody diluted at 1/1,000 (Sigma) and/or with anti-rhodopsin C9 antibody diluted at 1/300 (Abcam). Antibody dilutions and incubations were performed in 1× PBS containing 0.2% bovine serum albumin (BSA) and 0.05% Tween 20 for 1 h at room temperature. Cells were then washed three times with PBS-T, incubated with Alexa Fluor (AF) 488- or AF594-conjugated anti-mouse antibodies diluted at 1/2,000 (Invitrogen) for 1 h in the dark at room temperature, and washed three times. Cell monolayers were then visualized with a UV-light microscope (Carl Zeiss) after mounting of the coverslips using ProLong Gold antifade reagent containing 4′, 6-diamidino-2-phenylindole (Invitrogen) for nuclear DNA staining.

For promoter reporter assays, 5×10^6 EPC cells per well of 6-well plates were transfected (see above) with pIFNpro-LUC or pISREpro-LUC together with various plasmid DNA constructs. For ISRE promoter induction, EPC IFN1 was expressed in EPC cells (5×10^6 cells per well of a 6-well plate) by transfecting cells with 1 μg of pcDNA1-IFNepc (71). At 48 h posttransfection, supernatants were collected and clarified by centrifugation for 10 min at 1,800 × *g*. Supernatant aliquots diluted with GMEM at 1:4 were used to induce luciferase reporter expression driven by ISRE promoter in pISREpro-LUC-transfected EPC cells. Except under conditions where RIG-I Nter-eGFP was already included in the transfection mixture, a peGFP vector (1 μg) was added to normalize transfection efficiency between each condition. All transfection mixtures were adjusted with an empty vector (pcDNA) to contain an equal quantity of DNA plasmid. At 24 h or 48 h posttransfection, cell lysates were obtained by adding 300 μl of cell culture lysis reagent per well according to the manufacturer's instructions (luciferase reporter assay system; Promega). eGFP expression from peGFP or pRIG-I Nter-eGFP was measured from 100 μl of cell lysates on a Tecan Infinite M200 Pro reader using an excitation wavelength of 480 nm and an emission wavelength of 510 nm. Luciferase activity was then measured by adding 100 μl of luciferase assay reagent. Values of luciferase activities were normalized to the levels of eGFP fluorescence. The fold induction was calculated as the ratio of stimulated versus unstimulated (control) conditions.

Statistical analysis. Except for those in Fig. 9C and D, results shown in each figure were derived from at least three independent experiments; the data presented are means ± standard errors (SE), with the indicated *P* values of <0.05 (*), <0.01 (**), and <0.001 (***) considered significant. One-way comparisons were performed using analysis of variance (ANOVA) and Tukey's multiple-comparison test. In Fig. 9C, each time point was represented by two wells, and each virus titer determination was done in duplicate. Means and SE were calculated. Statistical significance was determined by multiple Student's *t* tests with the Sidak-Bonferroni correction method. In Fig. 9D, the standard deviations were calculated from triplicate experiments, and statistical significance was determined by unpaired *t* test. All analyses were performed using GraphPad Prism software version 6.0.

Coimmunoprecipitations, protein electrophoresis, and Western blot assays. For the coimmunoprecipitation assays, transfected EPC cells in 6-well plates were lysed at 72 h posttransfection using 300 μl of lysis buffer (150 mM NaCl, 50 mM Tris-HCl [pH 8], 20 mM ethylenediaminetetraacetic acid [EDTA], 0.5% NP-40, and complete protease inhibitor cocktail [Roche]). Aliquots of 200 μl were then incubated with 0.2 μg of rabbit anti-Flag M2 MAb (Sigma) or mouse anti-rhodopsin C9 antibody (Abcam) and protein A-Sepharose beads (GE Healthcare) were added. After extensive washes in Tris-buffered saline 1× (pH 7.5) containing 0.5% Tween 20, proteins were resuspended in 50 μl of cracking buffer 1× composed of 4% glycerol, 2% β-mercaptoethanol, 20 mM Tris (pH 7), 0.4% SDS, and bromophenol blue and then boiled.

For protein detection, transfected cells in 6-well plates were lysed at 48 h posttransfection using 100 μl of lysis buffer composed of 150 mM NaCl, 50 mM Tris-HCl (pH 8.5), 20 mM EDTA, 1% deoxycholic acid sodium salt (DOC), and 1% Triton X-100. Aliquots of 100 μl were then incubated with 25 μl of cracking buffer composed of 20% glycerol, 10% β-mercaptoethanol, 100 mM Tris (pH 7), 2% SDS, and bromophenol blue for 10 min in boiling water.

The samples were then separated by electrophoresis on a 4 to 12% gradient polyacrylamide bis-Tris gel (NuPage Novex; Invitrogen) followed by Western blot analysis. After electrotransfer onto a polyvinylidene difluoride (PVDF) membrane (Immobilon-P; Millipore), proteins were detected using either a mouse or a rabbit anti-Flag M2 MAb diluted to 1/500 (Sigma), a horseradish peroxidase (HRP)-conjugated rat anti-HA MAb diluted to 1/1,000 (Roche), a mouse anti-rhodopsin C9 antibody diluted to 1/1,000 (Abcam), or a mouse anti-alpha tubulin antibody diluted to 1/3,000 for loading controls (Sigma). Immunodetected antigens were visualized with HRP-conjugated goat anti-mouse or anti-rabbit antibody diluted to 1/5,000 (Seracare) using an enhanced chemiluminescence (ECL) detection system (Pierce), and antigen detection was performed using a ChemiDoc device (Bio-Rad).

SAV2 nsP2 template-based structural modeling and NLS prediction. The protein coding sequence of SAV2 nsP2 (nonstructural protein GenPept accession number CAC87660.1, from GenBank accession number AJ316246.1) was submitted to the RaptorX server (http://raptorx.uchicago.edu) for template-based protein structure homology modeling (73). RaptorX predicts the secondary and tertiary structures of proteins from an amino acid sequence of a query protein by performing quality assessment of protein homology alignments with one or multiple distantly related template proteins. For its structure predictions the server also makes use of a nonlinear scoring function and a probabilistic consistency algorithm. SAV2 nsP2 subdomain organization within the predicted helicase (N-domain and helicase) and protease (protease and C-domain) domains were delineated based on amino acid sequence alignment with the CHIKV nsP2 protein sequence (GenPept accession number ANH22474.1). The SAV2 structural model was visualized and annotated using the UCSF Chimera package (74).

Structural homology modeling of the nsP2 C-terminal domain (residues 624 to 857) was performed using the Phyre2 server (http://www.sbg.bio.ic.ac.uk/phyre2) (75). Phyre2 is based on an advanced multistage process involving a fold library scan using a hidden Markov model and a leading alignment algorithm (HHsearch). Phyre2 output provides a list of structural template hits with confidence scores allowing assessment of alignment coverage of predicted models, as well as the conserved functional and structural features of a query protein.

Nuclear localization signals within SAV2 nsP2 protein sequence were predicted using the cNLS Mapper server (http://nls-mapper.iab.keio.ac.jp/cgi-bin/NLS_Mapper_form.cgi), which accurately predicts nuclear localization signals specific to the conserved importin $\alpha\beta$ pathway by calculating the levels of NLS activities of each amino acid (39).

Putative DNA binding sites within the SAV2 nsP2 C-terminal domain were analyzed using the DisoRDPbind server (http://biomine.cs.vcu.edu/servers/DisoRDPbind/) (59). Protein regions displaying intrinsic disorder (i.e., lacking a stable three-dimensional structure) are often binding sites for biomolecules, in particular for DNA. DisoRDPbind performs accurate predictions of DNA binding sites using an efficient multilayered approach that utilizes information extracted from amino acid physiochemical properties, complexity of sequence, putative secondary structure and disorder, and sequence alignment. Additional DNA binding site analysis was performed using DP-Bind (http://lcg.rit.albany.edu/dp-bind/) (60). DP-Bind is based on three machine learning methods: support vector machine, kernel logistic regression, and penalized logistic regression. Sequence-based BLOSUM62 encoding was used in the analysis of the nsP2 C-terminal domain. The results output by the three methods are combined into a consensus prediction to help identify positions predicted with a high degree of confidence.

Generation of pSAV2 encoding nsP2 mutants. Using the pSAV2 infectious cDNA plasmid construct containing the full-length SAV2 cDNA as the template (40), a SpeI DNA fragment encompassing the complete nsP2 coding region was amplified by PCR with the 5SAV2SpeI and 3SAV2SpeI primers (Table 1) and cloned into the pJet1.2 vector (Thermo Fisher Scientific). nsP2 NLS domains were mutated by site-directed mutagenesis using a QuikChange site-directed mutagenesis kit (Stratagene) and specific primers (Table 1). All targeted mutations were verified by nucleotide sequencing. The mutated SpeI

fragments were cloned back into the SpeI-digested pSAV2 backbone, leading to pSAV2.ΔNLS1, pSAV2.ΔNLS2, and pSAV2.ΔNLS1 + 2. Mutated pSAV2 constructs (2 μg) were then transfected by electroporation (Amaxa Cell Line Nucleofector kit T and program T-006; Amaxa Biosystems) in BF-2 cells (5×10^6 cells per well in 6-well plates). Cells were incubated at 20°C overnight in 10% fresh medium. At 24 h posttransfection, the medium was replaced with serum-free fresh medium, and cells were incubated at 10°C for 14 days. Clarified supernatants were then used to infect fresh BF-2 cells. Viruses were detected by indirect immunofluorescence assays (see above).

RNA isolation and RT-qPCR analysis. CHSE-214 cells were infected at an MOI of 1 with rSAV2.WT or rSAV2.ΔNLS2 or mock-infected. At 96 h postinfection, total RNA was extracted using the RNeasy Plus minikit (Qiagen) and treated with DNase. The reverse transcription experiment was performed using the iScript advanced cDNA synthesis kit (Bio-Rad) according to the manufacturer's instructions. Gene expression was measured by real-time PCR with an Eppendorf RealPlex 2 qPCR real-time PCR ThermoCycler using iTaq Universal SYBR green supermix (Bio-Rad). Each sample was composed of 5 μl primers (5 μM each), 2 μl cDNA (diluted 1/2), and 10 μl PCR mastermix. Samples were first incubated at 95°C for 30 s, then subjected to 40 amplification cycles (95°C for 5 s and 60°C for 30 s), followed by the melting curve of PCR products from 65°C to 95°C with a 0.5°C increment every 5s. The relative fold induction of the gene of interest, normalized to an endogenous reference (elongation factor 1 alpha [EF1A]) and relative to a calibrator (mock-infected conditions) was determined using the comparative threshold cycle ($2^{-\Delta\Delta CT}$) method (76). All qPCR primers used in this study are shown in Table 1.

Data availability. The GenBank accession number for *Pimephales promelas* STAT1 is MN781136.

ACKNOWLEDGMENTS

We thank Sandra Souto and Alain Le Coupanec for helpful discussions.

This work was supported by the Institut de recherche pour l'agriculture, l'alimentation et l'environnement (INRAE). Raphaël Jami is the recipient of a Ph.D. fellowship from the Doctoral School ABIES, AgroParisTech.

R.J., J.K.M., and S.B. conceived and designed the experiments. R.J., E.M., J.B., and A.L. performed the experiments. R.J., J.K.M., and S.B. analyzed the data. R.J., J.K.M., and S.B. wrote the paper.

We declare no competing financial interests.

REFERENCES

1. Mérour E, Brémont M. 2014. Vaccination against diseases caused by salmonid alphavirus, p 334–340. In Gudding R, Lillehaug A, Evensen Ø (ed), Fish vaccination. John Wiley & Sons, Ltd., Chichester, UK.
2. OIE Aquatic Animal Health Standards Commission. 2019. Infection with salmonid alphavirus. In Manual of diagnostic tests for aquatic animals. World Organisation for Animal Health, Paris, France.
3. Villoing S, Bearzotti M, Chilmonczyk S, Castric J, Bremont M. 2000. Rainbow trout sleeping disease virus is an atypical alphavirus. J Virol 74:173–183. https://doi.org/10.1128/JVI.74.1.173-183.2000.
4. Weston J, Villoing S, Bremont M, Castric J, Pfeffer M, Jewhurst V, McLoughlin M, Rodseth O, Christie KE, Koumans J, Todd D. 2002. Comparison of two aquatic alphaviruses, salmon pancreas disease virus and sleeping disease virus, by using genome sequence analysis, monoclonal reactivity, and cross-infection. J Virol 76:6155–6163. https://doi.org/10.1128/JVI.76.12.6155-6163.2002.
5. Fringuelli E, Rowley HM, Wilson JC, Hunter R, Rodger H, Graham DA. 2008. Phylogenetic analyses and molecular epidemiology of European salmonid alphaviruses (SAV) based on partial E2 and nsP3 gene nucleotide sequences. J Fish Dis 31:811–823. https://doi.org/10.1111/j.1365-2761.2008.00944.x.
6. Button JM, Qazi SA, Wang JC, Mukhopadhyay S. 2020. Revisiting an old friend: new findings in alphavirus structure and assembly. Curr Opin Virol 45:25–33. https://doi.org/10.1016/j.coviro.2020.06.005.
7. Forrester NL, Palacios G, Tesh RB, Savji N, Guzman H, Sherman M, Weaver SC, Lipkin WI. 2012. Genome-scale phylogeny of the alphavirus genus suggests a marine origin. J Virol 86:2729–2738. https://doi.org/10.1128/JVI.05591-11.
8. Merour E, Lamoureux A, Bernard J, Biacchesi S, Bremont M. 2013. A fully attenuated recombinant salmonid alphavirus becomes pathogenic through a single amino acid change in the E2 glycoprotein. J Virol 87:6027–6030. https://doi.org/10.1128/JVI.03501-12.
9. Merour E, Lamoureux A, Biacchesi S, Bremont M. 2016. Fine mapping of a salmonid E2 alphavirus neutralizing epitope. J Gen Virol 97:893–900. https://doi.org/10.1099/jgv.0.000411.
10. Boscher SK, McLoughlin M, Le Ven A, Cabon J, Baud M, Castric J. 2006. Experimental transmission of sleeping disease in one-year-old rainbow trout, *Oncorhynchus mykiss* (Walbaum), induced by sleeping disease virus. J Fish Dis 29:263–273. https://doi.org/10.1111/j.1365-2761.2006.00716.x.
11. Biacchesi S, Jouvion G, Merour E, Boukadiri A, Desdouits M, Ozden S, Huerre M, Ceccaldi PE, Bremont M. 2016. Rainbow trout (Oncorhynchus mykiss) muscle satellite cells are targets of salmonid alphavirus infection. Vet Res 47:9. https://doi.org/10.1186/s13567-015-0301-1.
12. Jansen MD, Bang Jensen B, McLoughlin MF, Rodger HD, Taksdal T, Sindre H, Graham DA, Lillehaug A. 2017. The epidemiology of pancreas disease in salmonid aquaculture: a summary of the current state of knowledge. J Fish Dis 40:141–155. https://doi.org/10.1111/jfd.12478.
13. Reid KM, Patel S, Robinson AJ, Bu L, Jarungsriapisit J, Moore LJ, Salinas I. 2017. Salmonid alphavirus infection causes skin dysbiosis in Atlantic salmon (*Salmo salar* L.) post-smolts. PLoS One 12:e0172856. https://doi.org/10.1371/journal.pone.0172856.
14. Sommerset I, Walde CS, Bang Jensen B, Bornø B, Haukaas A, Brun E. 2020. The health situation in Norwegian aquaculture 2019. Norwegian Veterinary Institute, Ås, Norway.
15. Karlsen M, Gjerset B, Hansen T, Rambaut A. 2014. Multiple introductions of salmonid alphavirus from a wild reservoir have caused independent and self-sustainable epizootics in aquaculture. J Gen Virol 95:52–59. https://doi.org/10.1099/vir.0.057455-0.
16. Skjold P, Sommerset I, Frost P, Villoing S. 2016. Vaccination against pancreas disease in Atlantic salmon, *Salmo salar* L., reduces shedding of salmonid alphavirus. Vet Res 47:78. https://doi.org/10.1186/s13567-016-0362-9.
17. Thorarinsson R, Wolf JC, Inami M, Phillips L, Jones G, Macdonald AM, Rodriguez JF, Sindre H, Skjerve E, Rimstad E, Evensen O. 2021. Effect of a novel DNA vaccine against pancreas disease caused by salmonid alphavirus subtype 3 in Atlantic salmon (*Salmo salar*). Fish Shellfish Immunol 108:116–126. https://doi.org/10.1016/j.fsi.2020.12.002.
18. Langevin C, Boudinot P, Collet B. 2019. IFN signaling in inflammation and viral infections: new insights from fish models. Viruses 11 :302. https://doi.org/10.3390/v11030302.
19. Robertsen B. 2018. The role of type I interferons in innate and adaptive immunity against viruses in Atlantic salmon. Dev Comp Immunol 80:41–52. https://doi.org/10.1016/j.dci.2017.02.005.

20. Chen SN, Zou PF, Nie P. 2017. Retinoic acid-inducible gene I (RIG-I)-like receptors (RLRs) in fish: current knowledge and future perspectives. Immunology 151:16–25. https://doi.org/10.1111/imm.12714.
21. Poynter S, Lisser G, Monjo A, DeWitte-Orr S. 2015. Sensors of infection: viral nucleic acid PRRs in fish. Biology (Basel) 4:460–493.
22. Ke F, Zhang QY. 2019. Aquatic animal viruses mediated immune evasion in their host. Fish Shellfish Immunol 86:1096–1105. https://doi.org/10.1016/j.fsi.2018.12.027.
23. Onomoto K, Onoguchi K, Yoneyama M. 2021. Regulation of RIG-I-like receptor-mediated signaling: interaction between host and viral factors. Cell Mol Immunol 18:539–555. https://doi.org/10.1038/s41423-020-00602-7.
24. Ryman KD, Klimstra WB. 2008. Host responses to alphavirus infection. Immunol Rev 225:27–45. https://doi.org/10.1111/j.1600-065X.2008.00670.x.
25. Herath TK, Bron JE, Thompson KD, Taggart JB, Adams A, Ireland JH, Richards RH. 2012. Transcriptomic analysis of the host response to early stage salmonid alphavirus (SAV-1) infection in Atlantic salmon *Salmo salar* L. Fish Shellfish Immunol 32:796–807. https://doi.org/10.1016/j.fsi.2012.02.001.
26. Johansen LH, Thim HL, Jorgensen SM, Afanasyev S, Strandskog G, Taksdal T, Fremmerlid K, McLoughlin M, Jorgensen JB, Krasnov A. 2015. Comparison of transcriptomic responses to pancreas disease (PD) and heart and skeletal muscle inflammation (HSMI) in heart of Atlantic salmon (*Salmo salar* L). Fish Shellfish Immunol 46:612–623. https://doi.org/10.1016/j.fsi.2015.07.023.
27. Xu C, Guo TC, Mutoloki S, Haugland O, Evensen O. 2012. Gene expression studies of host response to salmonid alphavirus subtype 3 experimental infections in Atlantic salmon. Vet Res 43:78. https://doi.org/10.1186/1297-9716-43-78.
28. Sun B, Skjæveland I, Svingerud T, Zou J, Jørgensen J, Robertsen B. 2011. Antiviral activity of salmonid gamma interferon against infectious pancreatic necrosis virus and salmonid alphavirus and its dependency on type I interferon. J Virol 85:9188–9198. https://doi.org/10.1128/JVI.00319-11.
29. Xu C, Guo TC, Mutoloki S, Haugland O, Marjara IS, Evensen O. 2010. Alpha interferon and not gamma interferon inhibits salmonid alphavirus subtype 3 replication in vitro. J Virol 84:8903–8912. https://doi.org/10.1128/JVI.00851-10.
30. Merour E, Jami R, Lamoureux A, Bernard J, Bremont M, Biacchesi S. 2019. A20 (*tnfaip3*) is a negative feedback regulator of RIG-I-mediated IFN induction in teleost. Fish Shellfish Immunol 84:857–864. https://doi.org/10.1016/j.fsi.2018.10.082.
31. Garmashova N, Gorchakov R, Frolova E, Frolov I. 2006. Sindbis virus nonstructural protein nsP2 is cytotoxic and inhibits cellular transcription. J Virol 80:5686–5696. https://doi.org/10.1128/JVI.02739-05.
32. Garmashova N, Gorchakov R, Volkova E, Paessler S, Frolova E, Frolov I. 2007. The Old World and New World alphaviruses use different virus-specific proteins for induction of transcriptional shutoff. J Virol 81:2472–2484. https://doi.org/10.1128/JVI.02073-06.
33. Gorchakov R, Frolova E, Frolov I. 2005. Inhibition of transcription and translation in Sindbis virus-infected cells. J Virol 79:9397–9409. https://doi.org/10.1128/JVI.79.15.9397-9409.2005.
34. Ding MX, Schlesinger MJ. 1989. Evidence that Sindbis virus NSP2 is an autoprotease which processes the virus nonstructural polyprotein. Virology 171:280–284. https://doi.org/10.1016/0042-6822(89)90539-4.
35. Golubtsov A, Kaariainen L, Caldentey J. 2006. Characterization of the cysteine protease domain of Semliki Forest virus replicase protein nsP2 by *in vitro* mutagenesis. FEBS Lett 580:1502–1508. https://doi.org/10.1016/j.febslet.2006.01.071.
36. Hardy WR, Strauss JH. 1989. Processing the nonstructural polyproteins of sindbis virus: nonstructural proteinase is in the C-terminal half of nsP2 and functions both in *cis* and in *trans*. J Virol 63:4653–4664. https://doi.org/10.1128/JVI.63.11.4653-4664.1989.
37. Rausalu K, Utt A, Quirin T, Varghese FS, Zusinaite E, Das PK, Ahola T, Merits A. 2016. Chikungunya virus infectivity, RNA replication and non-structural polyprotein processing depend on the nsP2 protease's active site cysteine residue. Sci Rep 6:37124. https://doi.org/10.1038/srep37124.
38. Strauss EG, De Groot RJ, Levinson R, Strauss JH. 1992. Identification of the active site residues in the nsP2 proteinase of Sindbis virus. Virology 191:932–940. https://doi.org/10.1016/0042-6822(92)90268-t.
39. Kosugi S, Hasebe M, Tomita M, Yanagawa H. 2009. Systematic identification of cell cycle-dependent yeast nucleocytoplasmic shuttling proteins by prediction of composite motifs. Proc Natl Acad Sci U S A 106:10171–10176. https://doi.org/10.1073/pnas.0900604106.
40. Moriette C, Leberre M, Lamoureux A, Lai TL, Bremont M. 2006. Recovery of a recombinant salmonid alphavirus fully attenuated and protective for rainbow trout. J Virol 80:4088–4098. https://doi.org/10.1128/JVI.80.8.4088-4098.2006.
41. Fazakerley JK, Boyd A, Mikkola ML, Kaariainen L. 2002. A single amino acid change in the nuclear localization sequence of the nsP2 protein affects the neurovirulence of Semliki Forest virus. J Virol 76:392–396. https://doi.org/10.1128/jvi.76.1.392-396.2002.
42. Grieder FB, Davis NL, Aronson JF, Charles PC, Sellon DC, Suzuki K, Johnston RE. 1995. Specific restrictions in the progression of Venezuelan equine encephalitis virus-induced disease resulting from single amino-acid changes in the glycoproteins. Virology 206:994–1006. https://doi.org/10.1006/viro.1995.1022.
43. White LJ, Wang JG, Davis NL, Johnston RE. 2001. Role of alpha/beta interferon in Venezuelan equine encephalitis virus pathogenesis: effect of an attenuating mutation in the 5' untranslated region. J Virol 75:3706–3718. https://doi.org/10.1128/JVI.75.8.3706-3718.2001.
44. Fragkoudis R, Breakwell L, McKimmie C, Boyd A, Barry G, Kohl A, Merits A, Fazakerley JK. 2007. The type I interferon system protects mice from Semliki Forest virus by preventing widespread virus dissemination in extraneural tissues, but does not mediate the restricted replication of avirulent virus in central nervous system neurons. J Gen Virol 88:3373–3384. https://doi.org/10.1099/vir.0.83191-0.
45. Lemm JA, Rumenapf T, Strauss EG, Strauss JH, Rice CM. 1994. Polypeptide requirements for assembly of functional Sindbis virus replication complexes: a model for the temporal regulation of minus- and plus-strand RNA synthesis. EMBO J 13:2925–2934. https://doi.org/10.1002/j.1460-2075.1994.tb06587.x.
46. Gorchakov R, Frolova E, Sawicki S, Atasheva S, Sawicki D, Frolov I. 2008. A new role for ns polyprotein cleavage in Sindbis virus replication. J Virol 82:6218–6231. https://doi.org/10.1128/JVI.02624-07.
47. Schuchman R, Kilianski A, Piper A, Vancini R, Ribeiro JMC, Sprague TR, Nasar F, Boyd G, Hernandez R, Glaros T. 2018. Comparative characterization of the Sindbis virus proteome from mammalian and invertebrate hosts identifies nsP2 as a component of the virion and sorting nexin 5 as a significant host factor for alphavirus replication. J Virol 92:e00694-18. https://doi.org/10.1128/JVI.00694-18.
48. Bae S, Lee JY, Myoung J. 2020. Chikungunya virus nsP2 impairs MDA5/RIG-I-mediated induction of NF-κB promoter activation: a potential target for virus-specific therapeutics. J Microbiol Biotechnol 30:1801–1809. https://doi.org/10.4014/jmb.2012.12005.
49. Simmons JD, White LJ, Morrison TE, Montgomery SA, Whitmore AC, Johnston RE, Heise MT. 2009. Venezuelan equine encephalitis virus disrupts STAT1 signaling by distinct mechanisms independent of host shutoff. J Virol 83:10571–10581. https://doi.org/10.1128/JVI.01041-09.
50. Fros JJ, Liu WJ, Prow NA, Geertsema C, Ligtenberg M, Vanlandingham DL, Schnettler E, Vlak JM, Suhrbier A, Khromykh AA, Pijlman GP. 2010. Chikungunya virus nonstructural protein 2 inhibits type I/II interferon-stimulated JAK-STAT signaling. J Virol 84:10877–10887. https://doi.org/10.1128/JVI.00949-10.
51. Goertz GP, McNally KL, Robertson SJ, Best SM, Pijlman GP, Fros JJ. 2018. The Methyltransferase-like domain of Chikungunya virus nsP2 inhibits the interferon response by promoting the nuclear export of STAT1. J Virol 92[PMC] https://doi.org/10.1128/JVI.01008-18.
52. Akhrymuk I, Kulemzin SV, Frolova EI. 2012. Evasion of the innate immune response: the Old World alphavirus nsP2 protein induces rapid degradation of Rpb1, a catalytic subunit of RNA polymerase II. J Virol 86:7180–7191. https://doi.org/10.1128/JVI.00541-12.
53. White LK, Sali T, Alvarado D, Gatti E, Pierre P, Streblow D, Defilippis VR. 2011. Chikungunya virus induces IPS-1-dependent innate immune activation and protein kinase R-independent translational shutoff. J Virol 85:606–620. https://doi.org/10.1128/JVI.00767-10.
54. Frolov I, Garmashova N, Atasheva S, Frolova EI. 2009. Random insertion mutagenesis of Sindbis virus nonstructural protein 2 and selection of variants incapable of downregulating cellular transcription. J Virol 83:9031–9044. https://doi.org/10.1128/JVI.00850-09.
55. Breakwell L, Dosenovic P, Karlsson Hedestam GB, D'Amato M, Liljestrom P, Fazakerley J, McInerney GM. 2007. Semliki Forest virus nonstructural protein 2 is involved in suppression of the type I interferon response. J Virol 81:8677–8684. https://doi.org/10.1128/JVI.02411-06.
56. Cloutier N, Flamand L. 2010. Kaposi sarcoma-associated herpesvirus latency-associated nuclear antigen inhibits interferon (IFN) beta expression by competing with IFN regulatory factor-3 for binding to IFNB promoter. J Biol Chem 285:7208–7221. https://doi.org/10.1074/jbc.M109.018838.
57. Lefort S, Soucy-Faulkner A, Grandvaux N, Flamand L. 2007. Binding of Kaposi's sarcoma-associated herpesvirus K-bZIP to interferon-responsive

factor 3 elements modulates antiviral gene expression. J Virol 81:10950–10960. https://doi.org/10.1128/JVI.00183-07.
58. Fu YZ, Su S, Zou HM, Guo Y, Wang SY, Li S, Luo MH, Wang YY. 2019. Human cytomegalovirus DNA polymerase subunit UL44 antagonizes antiviral immune responses by suppressing IRF3- and NF-κB-mediated transcription. J Virol 93:e00181-19. https://doi.org/10.1128/JVI.00181-19.
59. Peng Z, Kurgan L. 2015. High-throughput prediction of RNA, DNA and protein binding regions mediated by intrinsic disorder. Nucleic Acids Res 43:e121. https://doi.org/10.1093/nar/gkv585.
60. Hwang S, Gou Z, Kuznetsov IB. 2007. DP-Bind: a web server for sequence-based prediction of DNA-binding residues in DNA-binding proteins. Bioinformatics 23:634–636. https://doi.org/10.1093/bioinformatics/btl672.
61. Biacchesi S, Merour E, Chevret D, Lamoureux A, Bernard J, Bremont M. 2017. NV proteins of fish novirhabdovirus recruit cellular PPM1Bb protein phosphatase and antagonize RIG-I-mediated IFN induction. Sci Rep 7:44025. https://doi.org/10.1038/srep44025.
62. Collet B, Secombes CJ. 2001. The rainbow trout (*Oncorhynchus mykiss*) Mx1 promoter: structural and functional characterization. Eur J Biochem 268:1577–1584. https://doi.org/10.1046/j.1432-1327.2001.02021.x.
63. Bergan V, Steinsvik S, Xu H, Kileng O, Robertsen B. 2006. Promoters of type I interferon genes from Atlantic salmon contain two main regulatory regions. FEBS J 273:3893–3906. https://doi.org/10.1111/j.1742-4658.2006.05382.x.
64. Sun F, Zhang YB, Liu TK, Shi J, Wang B, Gui JF. 2011. Fish MITA serves as a mediator for distinct fish IFN gene activation dependent on IRF3 or IRF7. J Immunol 187:2531–2539. https://doi.org/10.4049/jimmunol.1100642.
65. Thurmond S, Wang B, Song J, Hai R. 2018. Suppression of type I interferon signaling by flavivirus NS5. Viruses 10:712. https://doi.org/10.3390/v10120712.
66. Tay MY, Smith K, Ng IH, Chan KW, Zhao Y, Ooi EE, Lescar J, Luo D, Jans DA, Forwood JK, Vasudevan SG. 2016. The C-terminal 18 amino acid region of dengue virus NS5 regulates its subcellular localization and contains a conserved arginine residue essential for infectious virus production. PLoS Pathog 12:e1005886. https://doi.org/10.1371/journal.ppat.1005886.
67. Shah PS, Link N, Jang GM, Sharp PP, Zhu T, Swaney DL, Johnson JR, Von Dollen J, Ramage HR, Satkamp L, Newton B, Huttenhain R, Petit MJ, Baum T, Everitt A, Laufman O, Tassetto M, Shales M, Stevenson E, Iglesias GN, Shokat L, Tripathi S, Balasubramaniam V, Webb LG, Aguirre S, Willsey AJ, Garcia-Sastre A, Pollard KS, Cherry S, Gamarnik AV, Marazzi I, Taunton J, Fernandez-Sesma A, Bellen HJ, Andino R, Krogan NJ. 2018. Comparative flavivirus-host protein interaction mapping reveals mechanisms of dengue and Zika virus pathogenesis. Cell 175:1931–1945.e18. https://doi.org/10.1016/j.cell.2018.11.028.
68. Marazzi I, Ho JS, Kim J, Manicassamy B, Dewell S, Albrecht RA, Seibert CW, Schaefer U, Jeffrey KL, Prinjha RK, Lee K, Garcia-Sastre A, Roeder RG, Tarakhovsky A. 2012. Suppression of the antiviral response by an influenza histone mimic. Nature 483:428–433. https://doi.org/10.1038/nature10892.
69. Moriette C, LeBerre M, Boscher SK, Castric J, Bremont M. 2005. Characterization and mapping of monoclonal antibodies against the sleeping disease virus, an aquatic alphavirus. J Gen Virol 86:3119–3127. https://doi.org/10.1099/vir.0.81030-0.
70. Biacchesi S, Lamoureux A, Mérour E, Bernard J, Brémont M, 2010. Limited interference at the early stage of infection between two recombinant novirhabdoviruses: viral hemorrhagic septicemia virus and infectious hematopoietic necrosis virus. J Virol 84:10038–10050. https://doi.org/10.1128/JVI.00343-10.
71. Biacchesi S, LeBerre M, Lamoureux A, Louise Y, Lauret E, Boudinot P, Brémont M. 2009. Mitochondrial antiviral signaling protein plays a major role in induction of the fish innate immune response against RNA and DNA viruses. J Virol 83:7815–7827. https://doi.org/10.1128/JVI.00404-09.
72. Biacchesi S, Merour E, Lamoureux A, Bernard J, Bremont M. 2012. Both STING and MAVS fish orthologs contribute to the induction of interferon mediated by RIG-I. PLoS One 7:e47737. https://doi.org/10.1371/journal.pone.0047737.
73. Kallberg M, Wang H, Wang S, Peng J, Wang Z, Lu H, Xu J. 2012. Template-based protein structure modeling using the RaptorX web server. Nat Protoc 7:1511–1522. https://doi.org/10.1038/nprot.2012.085.
74. Pettersen EF, Goddard TD, Huang CC, Couch GS, Greenblatt DM, Meng EC, Ferrin TE. 2004. UCSF Chimera—a visualization system for exploratory research and analysis. J Comput Chem 25:1605–1612. https://doi.org/10.1002/jcc.20084.
75. Kelley LA, Mezulis S, Yates CM, Wass MN, Sternberg MJ. 2015. The Phyre2 web portal for protein modeling, prediction and analysis. Nat Protoc 10:845–858. https://doi.org/10.1038/nprot.2015.053.
76. Livak KJ, Schmittgen TD. 2001. Analysis of relative gene expression data using real-time quantitative PCR and the $2^{-\Delta\Delta}CT$ method. Methods 25:402–408. https://doi.org/10.1006/meth.2001.1262.